












Extreme Neutral Outflow in an Inactive Quenching Galaxy at $z \sim 1.3$ YANG SUN ¹, ZHIYUAN JI ¹, GEORGE H. RIEKE ¹, FRANCESCO D'EUGENIO ^{2,3}, YONGDA ZHU ¹, FENGWU SUN ⁴,
XIAOJING LIN ^{5,1}, ANDREW J. BUNKER ⁶, JIANWEI LYU (吕建伟) ¹, PIERLUIGI RINALDI ¹, AND
CHRISTOPHER N. A. WILLMER ¹¹*Steward Observatory, University of Arizona, 933 North Cherry Avenue, Tucson, AZ 85719, USA*²*Kavli Institute for Cosmology, University of Cambridge, Madingley Road, Cambridge, CB3 0HA, UK*³*Cavendish Laboratory, University of Cambridge, 19 JJ Thomson Avenue, Cambridge, CB3 0HE, UK*⁴*Center for Astrophysics | Harvard & Smithsonian, 60 Garden St., Cambridge MA 02138 USA*⁵*Department of Astronomy, Tsinghua University, Beijing 100084, China*⁶*Department of Physics, University of Oxford, Denys Wilkinson Building, Keble Road, Oxford OX1 3RH, UK***ABSTRACT**

We have discovered a substantial sodium doublet (Na D $\lambda\lambda 5890, 5896\text{\AA}$)-traced neutral outflow in a quenching galaxy JADES-GS-206183 at $z = 1.317$ in GOODS-S field. Its JWST NIRSpec/MSA spectrum shows a significantly blueshifted and deep Na D absorption, revealing a neutral outflow with a velocity of $v_{\text{out}} = 828^{+79}_{-49} \text{ km s}^{-1}$ and a mass outflow rate of $\log(\dot{M}_{\text{out}}/\text{M}_{\odot} \text{ yr}^{-1}) = 2.40^{+0.11}_{-0.16}$. The mass outflow rate of this outflow is higher than any of the neutral outflows identified previously beyond $z \sim 1$ by the same line diagnostic and is comparable with those in local galaxies with extremely strong star formation activities or luminous AGN. Nonetheless, the best-fit SED modeling of JADES-GS-206183, based on its multi-band photometry from HST/ACS to JWST/NIRCam, suggests that the host galaxy now is quenched, and the Paschen α (Pa α) emission in the FRESCO NIRCam grism spectrum confirms its current low star formation rate ($10.78 \pm 0.55 \text{ M}_{\odot} \text{ yr}^{-1}$). More surprisingly, optical line ratio diagnostics indicate that the current AGN activity of JADES-GS-206183, if present, is weak. Even though we tentatively detect a broad component of the H α line, it is more likely tracing the ionized outflow than an AGN. The results demonstrate that the Na D outflow in JADES-GS-206183 is highly unlikely to be driven by current star formation or nuclear activity. Instead, we propose that the outflow that we are witnessing in JADES-GS-206183 may be a long-lasting fossil outflow, powered by previous AGN activity that has recently shut down.

Keywords: Galactic Winds (572), Galaxy Evolution (594), Galaxy Quenching (2040), Star Formation (1569)

1. INTRODUCTION

Galactic outflows, as an essential step of the galactic baryon cycle, play a fundamental role in driving galaxy evolution, regulating star formation and central nuclear activities within a galaxy. Current cosmological simulations of galaxy formation and evolution invoke feedback to reproduce observed galaxy baryonic mass functions and star formation efficiency, and also to quench galaxies (Kereš et al. 2009; Hopkins et al. 2014; Somerville & Davé 2015; Naab & Ostriker 2017, and references

therein). Massive stars, supernovae, and active galactic nuclei (AGN), as the sources of outflows and thus feedback, transfer their own thermal or kinetic energy to the interstellar medium (ISM) in galaxies, heating or directly expelling ISM components outwards to suppress star formation and central nuclear activity.

From the observational perspective, many works have reported galactic outflows in both AGN hosts (e.g., Ciccone et al. 2014; Feruglio et al. 2015; Baron & Netzer 2019; Davies et al. 2020) and inactive galaxies (e.g., Heckman et al. 2000; Rupke et al. 2005a; Chen et al. 2010; Perrotta et al. 2021) in the local Universe over the past few decades. Specifically, many local post-starburst galaxies (PSB), whose star formation has shut

down in the past 1 Gyr (Dressler & Gunn 1983; Couch & Sharples 1987), commonly show outflow signatures. This behavior indicates that outflows should somehow contribute to galaxy quenching (e.g., Tremonti et al. 2007; Coil et al. 2011; Luo et al. 2022; Baron et al. 2022; Sun et al. 2024). Also, the outflows in PSBs are often multi-phase. Most of the PSB outflows are detected in a cool neutral phase through Na D absorption (Baron et al. 2022; Sun et al. 2024), but a large fraction of them also exhibit in the ionized phase traced by O III λ 5007, especially for those hosted by AGN-host PSBs. Additionally, Luo et al. (2022) reported a case of a quenching galaxy hosting outflows simultaneously in the ionized, neutral, and molecular phases.

Beyond the local Universe ($z > 1$), observations of PSB outflows using the same diagnostics as the local studies are challenging due to the limited wavelength coverage and sensitivities of pre-JWST facilities. Historically, the neutral phase outflows at higher redshift could only be studied using a UV absorption line (such as Si II λ 1304, 1636, Mg II λ 2796, 2804) because the more common optical tracer, Na D, is shifted to the infrared range. Also, the stacking approach was often applied to enhance the outflow signatures (e.g., Weiner et al. 2009; Steidel et al. 2010; Maltby et al. 2019), which prevents us from studying the outflow and its impact on host galaxy properties in single galaxies. Since JWST launched in 2021, many more high- z PSB galaxies have been spectroscopically discovered (e.g., Carnall et al. 2023; de Graaff et al. 2024). Also, an increasing number of outflows in the quenching galaxies have been detected at cosmic noon and beyond (Belli et al. 2024; Davies et al. 2024; D’Eugenio et al. 2024; Carniani et al. 2024; Zhu et al. 2024a; Wu 2025), which enables us to better understand the outflow and quenching mechanism in the early Universe. Among them, Belli et al. (2024) and D’Eugenio et al. (2024) detected the neutral outflows in two AGN-host PSBs through blueshifted Na D absorption at $z \sim 2.5$ and 3, respectively, for which the outflow mass rate is an order of magnitude higher than the current star formation rate of the hosts, indicating AGN-driven outflows can efficiently quench galaxies at high- z . In addition, a census of Na D outflows at cosmic noon from the JWST Cycle 1 Blue Jay survey (Davies et al. 2024; Park et al. 2024) shows that powerful neutral outflows are commonly detected in massive quenching systems, which seem to be powered by AGN activity. In short, the recent studies of Na D outflows in high- z PSBs all focus on galaxies with ongoing AGN activity, leading us to naturally link the nuclear activity to those outflows. However, since the lifetimes of AGN and outflows are not necessarily the same, we cannot

draw causality conclusions from comparing directly the relative incidence of the two. In particular, whether and how outflows are launched in the PSBs with quiet nuclear regions and how they impact galaxy quenching are still poorly understood at high- z .

In this work, we report the discovery of an extremely powerful Na D outflow in the $z \sim 1.3$ post-starburst galaxy JADES-GS-206183 (RA= 53.176589 deg, DEC= -27.785519 deg) without significant AGN signatures. The outstanding feature of this galaxy is that, even though its current star formation and AGN activity are weak, it surprisingly hosts a Na D outflow with the highest mass outflow rate detected so far beyond the local Universe, for which the outflow energy and mass rate are even comparable to the energetic outflows driven by local luminous starbursts or AGNs. Therefore, this galaxy gives crucial insight into the outflow launching mechanism and galaxy quenching around cosmic noon.

This paper is organized as follows: We present the data used in this study in Section 2, and then describe the spectral analysis and the SED modelling in Section 3 and 4, respectively. The results of outflows in JADES-GS-206183 and its host galaxy properties are shown in Section 5, and we discuss them in Section 6. Finally, we summarize our work in Section 7. Throughout this paper, we assume a standard Λ CDM universe whose cosmological parameters are $H_0 = 70 \text{ km s}^{-1} \text{ Mpc}^{-1}$, $\Omega_\Lambda = 0.7$, and $\Omega_m = 0.3$.

2. DATA

2.1. NIRSpec

We used JWST/NIRSpec Micro Shutter Assembly (MSA; Jakobsen et al. 2022; Ferruit et al. 2022) spectra from the SMILES survey (PID 1207, PI: Rieke; Albers et al. 2024; Rieke et al. 2024) to measure the properties of the Na D doublet ($\lambda\lambda$ 5890, 5896) in the spectrum of JADES-GS-206183. We observed with the G140M/F100LP and G235M/F170LP gratings and blocking filters to cover 0.97-3.07 μm in the observed frame (0.4-1.3 μm in the rest frame) at a spectral resolution of $R \sim 1000$. The effective exposure time with each disperser/filter combination was 7,000 seconds (~ 1.94 hours).

We processed and calibrated the data using the JWST Calibration Pipeline (Bushouse et al. 2022), version 1.14.0, with the CRDS¹ context `jwst.1236.pmap`. In brief, the `calwebb_detector1` stage converted “uncal.fits” files into uncalibrated rate images. Next, the `calwebb_spec2` stage applied flat-field corrections, flux

¹ Calibration Reference Data System: <https://jwst-crds.stsci.edu/>

calibration, and local background subtraction, yielding resampled spectra for each nodding position. The final spectral combination and extraction were carried out using `calwebb_spec3`. Additionally, we applied custom scripts to further reject hot pixels and remove $1/f$ noise. A detailed description of the reduction process, along with reduced spectra and the redshift catalog, will be provided in a forthcoming data release (Y. Zhu et al., in prep.; see also Zhu et al. 2024b). Given the extended morphology of JADES-GS-206183, we used only the two nodding positions (excluding the central position) for local background subtraction to avoid self-subtraction by the galaxy.

We also applied slit-loss corrections to the NIRSpec data, since the shutter covers only a fraction of the galaxy. We calculated F115W and F210M synthetic photometry from the spectrum (the two filters avoid strong emission lines) and then determined the correction factors for the two bands by comparing them with the corresponding KRON convolved NIRCам photometry from the JADES v1.0 photometric catalog. We then did a linear interpolation between the two band correction factors to globally correct the whole spectrum. We confirm the slit-loss corrected NIRSpec spectrum matches the best-fit SED derived from multi-band photometry (Section 4).

2.2. NIRCам

We obtained photometry in 13 wide- and medium-band NIRCам filters (F090W, F115W, F150W, F182M, F200W, F210M, F277W, F356W, F410M, F430M, F444W, F460M and F480M) of JADES-GS-206183, as well as legacy HST photometric data in the ACS/WFC filters (F435W, F606W, F775W, F814W and F850LP) and in the WFC3 filters (F105W, F125W, F140W, and F160W) from the JADES catalog (Rieke et al. 2023b, with updates to the photometry in Eisenstein et al. 2023a,b; D’Eugenio et al. 2025 and JADES Collaboration, in prep.). HST/ACS, HST/WFC3 and JWST/NIRCам filters together nicely cover the rest-frame optical to near-IR spectral energy distributions (SEDs) of the galaxy, allowing reasonable constraints on its stellar properties. In addition, to better reveal the morphological structure, we derived false-color RGB imaging using F115W/F200W/F356W, which is shown in the top left panel of Figure 1. The RGB image of JADES-GS-206183 shows structures that are morphologically identical to a bar, with spiral arms emanating from both ends. The bar length is about 0.6 arcsec (~ 10 kpc), comparable with the effective radius of the galaxy. Given this large bar size, observed in a quiescent galaxy

at $z > 1$, we remark that kinematic confirmation would be needed.

JADES-GS-206183 also has spectroscopic data obtained with JWST/NIRCам Wide Field Slitless Spectroscopy (WFSS) from the FRESCO survey (Oesch et al. 2023) in the F444W band ($\lambda \sim 3.9\text{--}5.0 \mu\text{m}$). The FRESCO survey covers a $7.4' \times 8.4'$ area in both GOODS fields with the row-direction grisms on both modules of JWST/NIRCам providing a spectral resolution of $R \sim 1590\text{--}1680$ from 3.9 to $5.0 \mu\text{m}$. The 5σ line sensitivity of FRESCO is $2 \times 10^{-18} \text{ erg s}^{-1} \text{ cm}^{-2}$.

The NIRCам/WFSS data was processed by the publicly available reduction routine presented in Sun et al. (2023)². We first processed the NIRCам data through the standard JWST stage-1 calibration pipeline³ v1.11.2. We assigned world coordinate system (WCS) information for the grism, performed flat-fielding, and removed the σ -clipped median sky background. The WCS of the grism exposure is registered to Gaia DR3 (Gaia Collaboration et al. 2023) using the NIRCам short-wavelength imaging data taken at the same time. For JADES-GS-206183, we extracted the 2D spectrum from individual grism exposures, and coadded them in a common wavelength (1 nm/pixel) and spatial ($0''.06/\text{pixel}$) grid. Prior to our scientific spectral extraction, we also extracted spectra of bright point sources ($\lesssim 21$ AB mag) to ensure the accuracy of the spectral tracing function and spectral flux calibration. We also extracted the spectrum of the galaxies with known ground-based spectroscopic redshifts, measuring the line center of detected Paschen α and β lines to ensure the wavelength calibration error at < 1 nm. We then optimally extracted the 1D spectrum of our target JADES-GS-206183 from coadded 2D spectrum using the surface brightness profile in the F444W band (Horne 1986), for which the integrated flux perfectly matches the F444W photometry.

3. SPECTROSCOPIC ANALYSIS

3.1. Stellar Continuum Modeling and Optical Emission Line Fitting

Both stellar absorption and the ISM can contribute to Na D absorptions; therefore, we first model the stellar continuum of the JADES-GS-206183 in its NIRSpec G140M and G235M spectra, using the penalized pixel fitting (pPXF, Cappellari & Emsellem 2004; Cappellari 2017, 2023) Python code. pPXF allows us to model the stellar continuum with a non-linear χ^2 minimization in

² <https://zenodo.org/records/14052875> (Sun 2024)

³ <https://zenodo.org/records/8140011> (Bushouse et al. 2024)

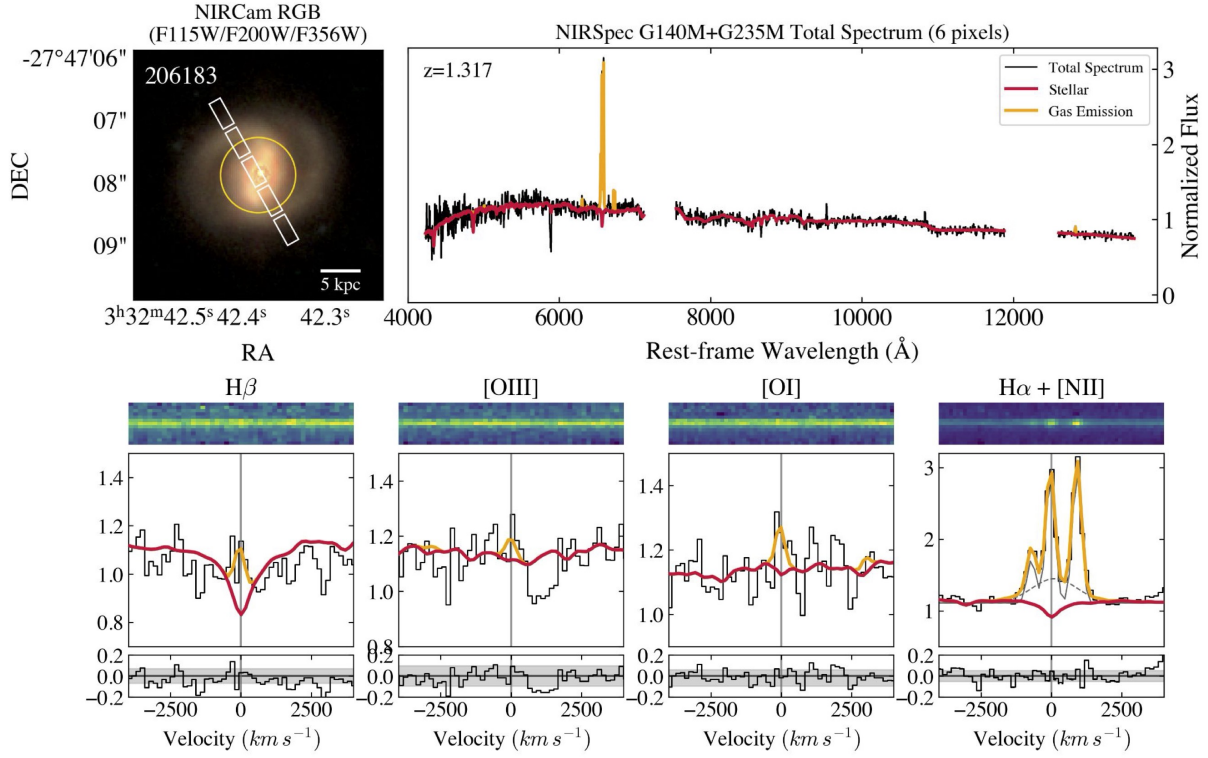


Figure 1. JWST observations of JADES-GS-206183. **Top left:** NIRCcam false-color RGB image generated from the F115W/F200W/F356W images overlaid with the position of the NIRSpect MSA shutters and the yellow circle representing the galaxy effective radius (0.6 arcsec). **Top right:** NIRSpect MSA G140M and G235M spectrum (black), the best-fit stellar continuum from pPXF (red), and the nebular emission (orange). The two spectral gaps are caused by the NIRSpect detector gap. **Bottom:** From left to right, the zoom-in original 2D spectra (top), best-fits (middle), residuals (bottom) of $H\beta$, $[O\text{III}]\lambda 5007$, $[O\text{I}]\lambda 6300$ and $H\alpha + [N\text{II}]\lambda\lambda 6548, 6584$. In the $H\alpha + [N\text{II}]$ panel, the narrow and additional broad components are shown by the gray solid and dashed lines, respectively. The averaged 1σ noise levels are also plotted in the residual panels.

the galaxy spectrum, at the same time taking into account the instrument line spread function (LSF). In our modeling, we adopt the LSF from [Jakobsen et al. \(2022\)](#).

We build the stellar templates using the Flexible Stellar Population Synthesis (FSPS; [Conroy et al. 2009; Conroy & Gunn 2010](#)) model built by [Cappellari \(2023\)](#), with the MILES stellar spectral library ([Sánchez-Blázquez et al. 2006; Falcón-Barroso et al. 2011](#)), the MIST isochrones ([Choi et al. 2016](#)) and the Salpeter IMF ([Salpeter 1955](#))⁴. The templates span a logarithmically spaced grid of ages and metallicities, covering the range of 1 Myr–15.85 Gyr with 0.1 dex sampling and $[Z/H] = -1.75$ –0.25 with 0.25 dex sampling, respectively. We limit the age of the input templates to no longer than the Universe age at the redshift of JADES-GS-206183 (4.68 Gyr).

⁴ Even though we use the Salpeter IMF here, which is inconsistent at the lower mass end compared to other widely-used IMFs, i.e. the Kroupa IMF that we use for SED fitting (see Section 4), [Cappellari \(2023\)](#) confirmed the pPXF spectral fitting result is insensitive to the slope of the IMF at low masses.

In pPXF fitting, we mask the nebular emission lines, including Balmer lines, $[O\text{III}]\lambda\lambda 4959, 5007$, $[O\text{I}]\lambda 6300$, $[N\text{II}]\lambda\lambda 6548, 6584$, and $[S\text{II}]\lambda\lambda 6717, 6731$. We will independently fit the profiles and calculate the fluxes of those emission lines after subtracting the stellar continuum derived by pPXF in the next section. We confirm the best-fit stellar continuum is not affected by whether the nebular emission lines are simultaneously fitted or not. The Na D line is also masked in our modeling⁵. Finally, a fourth-degree multiplicative polynomial is used to avoid mismatches between galaxy spectra and stellar templates and to ensure the accuracy of the fitted kinematic parameters.

We first run pPXF by assuming the systemic redshift of JADES-GS-206183 to be the same as that derived from emission line measurements obtained with ALMA and VLT/MUSE ([Inami et al. 2017; Boogaard et al. 2019](#)). After obtaining the first pPXF results for stellar

⁵ We confirm masking the Na D region or not does not have impact on the best-fit stellar model around Na D and the further Na D-derived ISM properties

kinematics, we adjust the redshift of JADES-GS-206183 using the stellar velocity and re-ran the pPXF fitting. The pPXF fitting results are shown in the top right panel of Figure 1. The spectrum displays stellar absorption features, in line with the typical spectral features observed in quiescent/post-starburst galaxies (e.g., Park et al. 2024).

Next, we model the pure nebular emission features using the Python package `lmfit` on the stellar continuum-subtracted spectrum. A single Gaussian profile is assigned for Balmer lines, [O III] $\lambda\lambda 4959, 5007$, [O I] $\lambda 6300$, [N II] $\lambda\lambda 6548, 6584$, and [S II] $\lambda\lambda 6717, 6731$, which shares the same velocity and velocity dispersion. The line width of the narrow component is limited within 300 km s^{-1} . For $H\alpha$, we add a broad Gaussian profile to the narrow component, which may be present due to outflows and/or AGN activity. For the broad components in our modeling, the width is allowed to vary between $300 - 5000 \text{ km s}^{-1}$. We test the necessity of this broad component using the Bayesian information criterion (BIC) method. We calculate BIC parameters for the “narrow-only” and “narrow+broad” models, and define the detection of a broad component where the difference of BIC between the “narrow-only” and “narrow+broad” model is larger than 10 ($\Delta\text{BIC} = \text{BIC}_n - \text{BIC}_{n+b} > 10$). Finally, we used a bootstrap approach to derive the uncertainties of the line profile parameters and fluxes.

The best-fit emission line profiles are shown in Figure 1. JADES-GS-206183 only exhibits low-ionization nebular lines (e.g., $H\alpha$, [N II], [S II]), lacking high-ionization emission lines, e.g. [O III] (see zoom-in line fittings in the bottom row of Figure 1). The line fluxes and stellar and gas kinematics properties are shown in Table 1. The gas velocity (relative to the stellar component) is -27 km s^{-1} , much smaller than the instrumental velocity dispersion ($\sim 100 \text{ km s}^{-1}$), suggesting that the narrow component of the emission lines is tracing gas well coupled with the stellar component. The gas velocity dispersion is in good agreement with the stellar one derived by pPXF, about $\sim 100 \text{ km s}^{-1}$.

In addition, the BIC difference between the “narrow-only” and “narrow+broad” model is larger than 10 ($\Delta\text{BIC} > 10$), suggesting that an additional broad component with a FWHM of $\sim 2000 \text{ km s}^{-1}$ is needed to reproduce the spectral range of $H\alpha + [\text{N II}]$ well (the bottom right panel of Figure 1), and thus the presence of additional gas component(s) with distinct kinematics in JADES-GS-206183. In Section 5.3, we will discuss the possible origin(s) of this broad gas component.

3.2. Na D Absorption Line Fitting

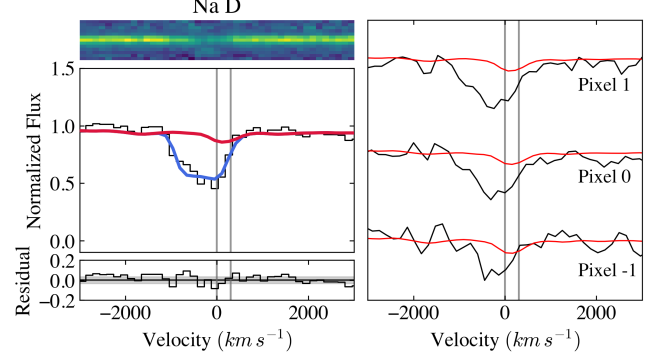


Figure 2. **Left:** Best-fit Na D profile of JADES-GS-206183. The top panel shows the original 2D MSA spectrum. In the middle panel, the black, red, and blue lines show the 1D MSA spectrum extracted from a 6-pixel-wide aperture, the best-fit stellar continuum by pPXF, and the best-fit ISM Na D absorption, respectively. The two gray vertical lines illustrate the systemic velocity of Na D $\lambda 5890, 5896$. The bottom panel displays the fitting residual. **Right:** Row-by-Row spectra of the central three rows of the JADES-GS-206183 spectrum. We label the rows with 1, 0, and -1 from top to bottom.

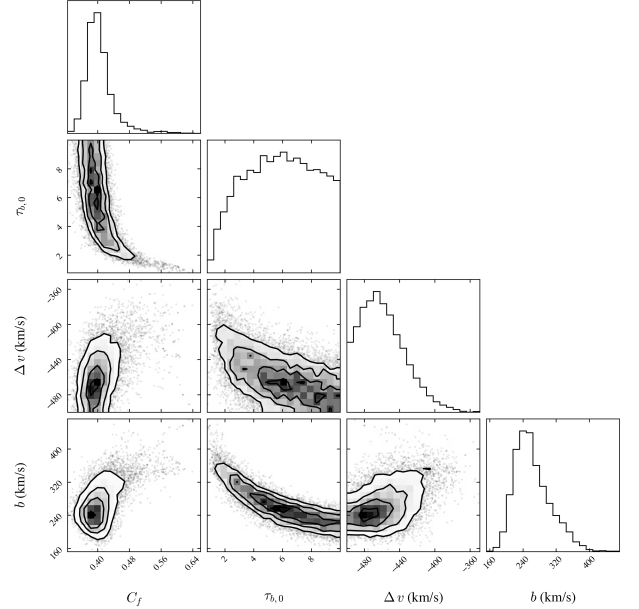


Figure 3. MCMC posterior parameter distributions and best-fits of Na D profile parameters (C_f , $\tau_{b,0}$, Δv , and b).

After obtaining the stellar Na D contribution from pPXF, we are then able to model the part of the Na D absorption arising from the ISM.

We fit the Na D line profile as:

$$F(\lambda) = F_* \times F_{\text{Na D, ISM}}, \quad (1)$$

Component		Δv (km s ⁻¹)	FWHM (km s ⁻¹)	Flux (10 ⁻¹⁷ erg s ⁻¹ cm ⁻²)
star		0 ± 5	245 ± 57	
H β		-31 ± 19	223 ± 28	0.54 ± 0.10
[O III] λ 5007		-31 ± 19	223 ± 28	0.15 ± 0.11
[O I] λ 6300		-31 ± 19	223 ± 28	0.33 ± 0.09
H α	narrow	-28 ± 5	193 ± 35	3.31 ± 0.44
	broad	-150 ± 60	843 ± 154	2.02 ± 0.55
[N III] λ 6584	narrow	-28 ± 5	193 ± 35	3.19 ± 0.45
	broad	-100 ± 43	940 ± 169	2.25 ± 0.40
[S II] λ 6717&6731	narrow	-28 ± 5	193 ± 35	0.44 ± 0.21
	broad	-100 ± 43	940 ± 169	1.14 ± 0.30
Pa α		-4 ± 6	213 ± 17	1.67 ± 0.08

Table 1. The kinematic properties (velocity and dispersion) of star and gas traced by multiple emission lines in JADES-GS-206183. The properties of [O III], H β , [O I], and Pa α were derived using a single Gaussian component, while for the H α , [N II] and [S II], the properties were estimated through multiple Gaussian components (5.3).

where F_* is the stellar continuum derived from pPXF and $F_{\text{Na D, ISM}}$ is the ISM Na D absorption. $F_{\text{Na D, ISM}}$ is parametrized using the standard partial covering model from Rupke et al. (2005a):

$$F_{\text{Na D, ISM}}(\lambda) = 1 - C_f + C_f e^{(-\tau_b(\lambda) - \tau_r(\lambda))}, \quad (2)$$

where C_f is the covering fraction of the foreground absorbing gas against the background continuum source, τ_b and τ_r are the optical depths of the blue (5891Å) and red (5897Å) Na D lines, respectively. For Na D, $\tau_b/\tau_r = 2$. The optical depth is modeled by a Gaussian profile:

$$\tau(\lambda, b) = \tau_0 e^{-(\lambda - \lambda_0)^2 / (\lambda_0 b / c)^2}, \quad (3)$$

where λ_0 is the central wavelength of the line, b is the Doppler width convolved with the instrumental dispersion, and c is the speed of light. With our spectral resolution of $R \sim 1000$, the He I λ 5877 emission would be blended with Na D. Therefore, in total, the four parameters of the Na D line model are λ_0 , τ_b , b , and C_f .

As many previous works cautioned, the absorption optical depth and covering fraction are degenerate when the Na D lines are blended (Rupke et al. 2005a; Davies et al. 2024). To properly account for this degeneracy and hence to better estimate the parameter uncertainties, we adopt the Markov Chain Monte Carlo (MCMC) method using emcee (Foreman-Mackey et al. 2013a) for the fitting procedure.

The best-fit line parameters and their uncertainties are shown in Figure 3, and the final best-fit ISM Na D profile is shown by the blue lines in the left panel of Figure 2. The ISM Na D component is significantly blueshifted ($\Delta v = -459_{-24}^{+28}$ km s⁻¹) from the stellar component (i.e. the systemic velocity), indicating that

the Na D-traced neutral phase ISM is outflowing in JADES-GS-206183.

The spectra of JADES-GS-206183 were extracted using a 6-pixel aperture (with a pixel size of 0.1"). However, as shown in the top left panel of Figure 1, JADES-GS-206183 exhibits an elongated substructure near its center in the NIRCcam imaging – presumably a stellar bar. This elongated structure is oriented at approximately ~ 20 degrees from the north and is not well aligned with the orientation of the MSA shutter. As a result, the position of the flux centroid varies across the shutter. Since this effect is not accounted for in our spectral extraction procedure, it may artificially broaden the NaD absorption feature.

To investigate this, we extracted six spectra pixel by pixel. We find only the spectra of the central three pixels – one from the center and two from positions one pixel above and below the center – show a clear Na D feature. We then used pPXF to model the three spectra independently (right panel of Figure 2). We find that the Na D feature is significantly blueshifted in all three spectra. Moreover, the total strength of the ISM Na D absorption calculated by co-adding the fitting results of the three spectra is almost identical to that obtained from fitting the original combined spectrum extracted with a 6-pixel aperture. These results suggest that the blueshifted and strong Na D absorption measured using the single combined spectrum is robust.

Interestingly, we note that the strength of the Na D absorption is stronger in the spectrum extracted from one pixel above the center (the top spectrum in the right panel of Figure 11) compared to the spectrum extracted from one pixel below the center (the bottom one). This suggests that the Na D outflow is preferentially originating from the upper-left (i.e., north-east)

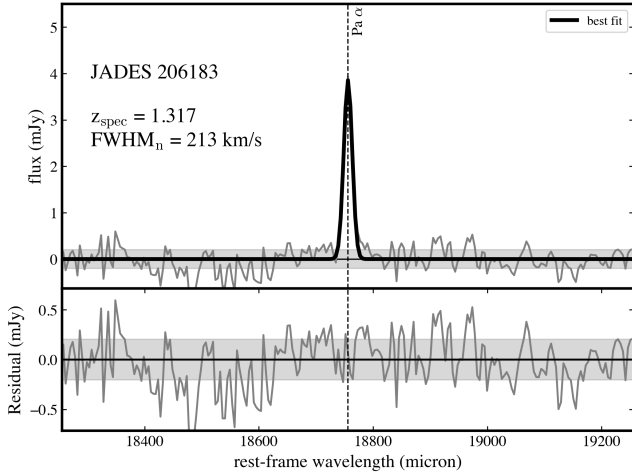


Figure 4. Line profile fitting for the Pa α . We show the extracted 1D spectrum (stellar continuum subtracted) and 1σ error level (grey line and shading), and the best-fit line profile (black).

region of JADES-GS-206183. As we will present in Section 3.4, we also observe possible evidence of an ionized outflow in the same direction based on the morphology of [OII] emission from MUSE observations of JADES-GS-206183.

3.3. Pa α

We estimated the SFR of JADES-GS-206183 using the Paschen α (Pa α) emission in its FRESCO grism spectrum. Compared to other commonly-used SFR indicators, e.g., H α , Pa α is a more accurate SFR tracer because it is substantially less affected by dust attenuation.

We first model the stellar continuum of the FRESCO spectrum using the same method as we introduced in Section 3.1 to estimate the contribution of the stellar Pa α absorption using pPXF. We mask Pa α during pPXF fitting. We fix the stellar kinematics to the pPXF results of the NIRSspec spectrum because the continuum is not well detected in the grism results. We subtract the stellar continuum from the original spectrum and then apply single/double Gaussian profiles to model the Pa α emission using `lmfit`. Given that the H α from JADES-GS-206183 shows a broad component (Section 3.1), we also test the necessity of a broad component for Pa α using the BIC method. We find that the BIC of the “narrow+broad” case is even larger than the narrow-only case ($\Delta\text{BIC} = -5$), indicating Pa α only needs a narrow component. The final best-fit of Pa α is shown in Figure 4. The observed Pa α flux is $1.68 \pm 0.08 \times 10^{-17} \text{ erg s}^{-1} \text{ cm}^{-2}$; and its intrinsic width is $213 \pm 17 \text{ km s}^{-1}$, consistent with the width of the nar-

row component of the emission lines detected in the $R \sim 1000$ NIRSspec spectrum.

With H α (details of the measurement process will be presented in Section 5.3) and Pa α , we derive the gas reddening (A_V) using the Balmer decrement method⁶ and the Calzetti et al. (2000) dust attenuation law. Given that the total H α profile contains a broad outflow component, we only use the narrow H α flux here to calculate the attenuation. Under Case B recombination (and assuming $T_e = 10^4 \text{ K}$ and $n_e = 100 \text{ cm}^{-3}$), the intrinsic flux ratio between H α and Pa α is 8.13 Osterbrock & Ferland (2006). The observed flux ratio of 1.98 ± 0.28 , corresponding to a gas reddening A_V of 2.27 ± 0.23 magnitude. After correcting for the dust attenuation using the A_V , we derive the intrinsic Pa α line luminosity, which is $2.34 \pm 0.11 \times 10^{41} \text{ erg s}^{-1}$.

Finally, using the Pa α -SFR relation from Neufeld et al. (2024) which is based on the (Chabrier 2003) IMF:

$$\text{SFR} (\text{M}_{\odot} \text{ yr}^{-1}) = 4.6 \times 10^{-41} \times L(\text{Pa}\alpha) (\text{erg s}^{-1}), \quad (4)$$

we obtain a $\text{SFR}_{\text{Pa}\alpha}$ of $10.78 \pm 0.55 \text{ M}_{\odot} \text{ yr}^{-1}$. JADES-GS-206183 is ~ 0.6 dex below the star forming galaxy main sequence at $z \sim 1.5$ (with a scatter of 0.3-0.4 dex) Leja et al. (2022), confirming its quiescent/PSB nature.

3.4. [OII] $\lambda\lambda 3726, 3729$ map

We use VLT/MUSE data for JADES-GS-206183 acquired by the MUSE Hubble Ultra-Deep Field survey from AMUSED⁷. Specifically, JADES-GS-206183 was covered by the MXDF – a part of the MUSE HUDF survey. The details of MUSE data reduction and AMUSED data products can be found in Bacon et al. (2023).

We study the spatial distribution of [O II] $\lambda\lambda 3726\&3729$ – the only strong emission line detected in the MUSE data for JADES-GS-206183. The full 1D spectrum is shown in Figure 5. To obtain the [O II] map, we derive the [O II] $\lambda\lambda 3726\&3729$ flux in each spaxel by integrating the fluxes within the rest-frame wavelength range of $[3721, 3735] \text{ \AA}$ after subtracting the average of the adjacent continuum.

The white light stellar continuum image along with the contours of [O II] flux derived from the MUSE data for JADES-GS-206183 is shown in Figure 5. Relative to the stellar continuum, the [O II] emission appears to lie toward the upper-left of the galaxy, suggesting a possible ionized outflow (traced by [O II]) in JADES-GS-206183. Notably, this direction also coincides with the observed

⁶ We do not adopt the traditional H β /H α method because the flux measurement of H β is relatively uncertain since its apparent emission is reduced by the stellar absorption.

⁷ <https://amused.univ-lyon1.fr/project/UDF/>

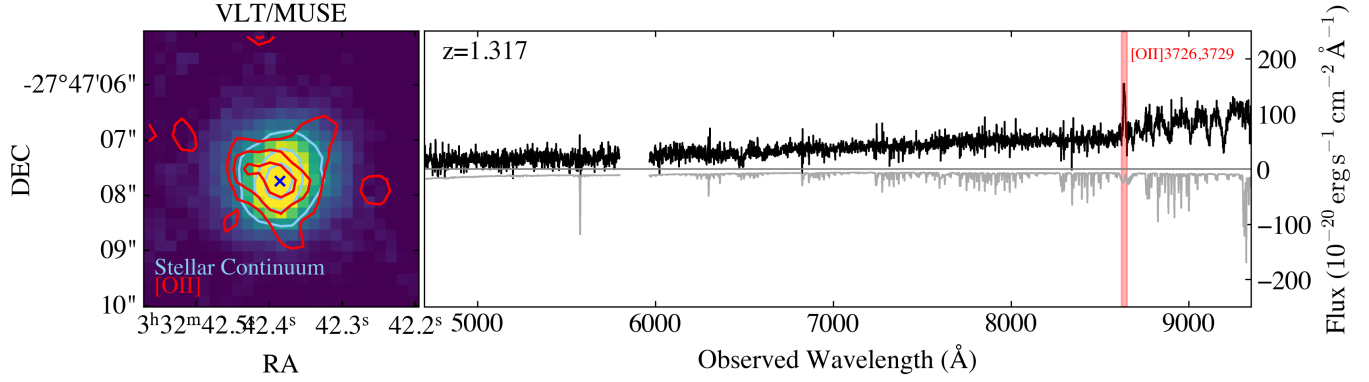


Figure 5. MUSE observation of JADES-GS-206183. **Left:** The AMUSED $5'' \times 5''$ white light map tracing stellar continuum light with the blue contour level of 10σ , 20σ , and 30σ . The blue cross marks the center of the stellar emission. The contour of $[\text{OII}]\lambda\lambda 3726, 3729$ with levels of 1σ , 1.5σ and 2σ (red) is overlaid on the above. **Right:** The integrated 1D spectrum (black) extracted based on the Rafelski segmentation map (Rafelski et al. 2015) and the corresponding flux uncertainties (gray). The red-shaded region represents the integrated spectral window for mapping the $[\text{OII}]$ emission.

Na D outflow (Section 3.2), indicating that, if real, the ionized outflow may be coupled with the neutral gas outflow. However, given that the MUSE observation of JADES-GS-206183 was conducted with a seeing limit of $\sim 0.8''$, we emphasize that no definitive conclusions can be drawn at this stage from the MUSE observation regarding the presence of an ionized outflow in JADES-GS-206183.

4. SED MODELLING

We infer the stellar population properties of JADES-GS-206183 via SED fitting with Prospector (Johnson et al. 2021) using photometry from a total of 22 filters, including HST/ACS and WFC3, and JWST/NIRCam.

Our SED assumptions, including parameter priors, are similar to those used in Ji et al. (2024). In brief, we fix the redshift to the spectroscopic redshift by pPXF ($z = 1.317$). We use the Kroupa stellar IMF (Kroupa 2001), and adopt the FSPS stellar synthesis code (Conroy et al. 2009; Conroy & Gunn 2010) with the stellar isochrone libraries MIST (Choi et al. 2016) and the MILES stellar spectral libraries (Sánchez-Blázquez et al. 2006; Falcón-Barroso et al. 2011). We use the Madau IGM transmission model (Madau 1995). We include the nebular emission model from Byler et al. (2017). We set the stellar metallicity (Z_*), the gas metallicity (Z_{gas}), and the ionization parameter (U) as free parameters. We use a two-component dust attenuation model, where the attenuation toward nebular emission and young (< 10 Myr) stellar populations are modeled by a power law, and towards old (> 10 Myr) stellar populations are treated following the parameterization of Noll et al. (2009), a modified Calzetti et al. (2000) law with the 2175\AA dust feature.

For the fiducial star formation history (SFH), we use a nonparametric, piece-wise form composed of 9 lookback time bins with the Dirichlet prior (Leja et al. 2017). The first three lookback time bins are fixed to be $0 - 10$, $10 - 30$ and $30 - 100$ Myr to capture recent episodes of star formation with relatively high time resolution. The last lookback time bin is $0.9t_H - t_H$ where t_H is the Hubble Time at $z = 1.317$. The remaining five bins are evenly spaced in logarithmic space between 100 Myr and $0.9t_H$. We also test another commonly-used continuity prior for the non-parametric SFH (Leja et al. 2019). We do not see any substantial changes in the SED properties of JADES-GS-206183 derived from these two different priors.

The best-fit SED and the reconstructed SFH derived from the fiducial Prospector model with the Dirichlet prior are shown in Figure 6, respectively. The model SED shows a strong rest-frame 4000\AA break and prominent absorption features associated with A-type stars, in agreement with the stellar continuum captured in the SMILES NIRSpec spectra (Figure 1). The inferred stellar mass of JADES-GS-206183 is $\log(M_*/M_\odot) = 11.15^{+0.04}_{-0.05}$ and its SED-derived current star formation rate is $\text{SFR}_{\text{SED}} = 7.5^{+4.1}_{-2.1} M_\odot \text{yr}^{-1}$. The SED-inferred SFR is within 1σ of the Pa α -derived SFR, supporting the robustness of the SED modeling result. In addition, the SED fit shows that a stellar-only model can already reproduce the multi-band observed photometry, suggesting there is no hint of a strong ongoing AGN in JADES-GS-206183. We will present and discuss other evidence against an AGN in Section 5.3. The reconstructed SFH displayed in the right panel of Figure 6 illustrates that JADES-GS-206183 experienced a starburst ~ 1 Gyr ago. By the time of observation, the star formation activity of JADES-GS-206183 is at a very low level with a sSFR

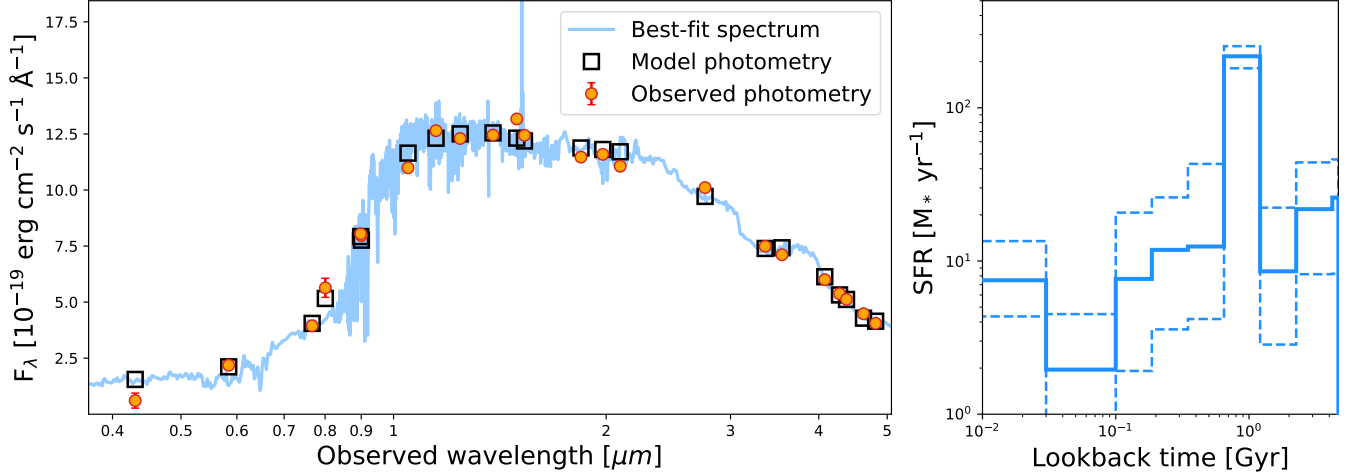


Figure 6. **Left:** The best-fit SED (blue line) of JADES-GS-206183 assumed the Dirichlet prior. The orange points show the observed HST/ACS and JWST/NIRCam photometry, and the black squares are the model photometry. **Right:** Reconstructed nonparametric SFH of JADES-GS-206183 (solid line). The 1σ uncertainties are plotted as dashed lines.

of only $\log(\text{sSFR}/\text{yr}^{-1}) \sim -10.6$ (-10.1 if adopt the $\text{SFR}_{\text{Pa}\alpha}$).

5. RESULTS

5.1. Physical properties of the Na D outflow

Our SMILES NIRSpec spectroscopy reveals the presence of a substantial outflow of neutral gas in JADES-GS-206183, as traced by Na D absorption which is blueshifted by -459 km s^{-1} (Section 3.2). With modeling results for the Na D line presented in this section, we further measure the physical properties of this neutral outflow in JADES-GS-206183.

In particular, we derive the outflow velocity (v_{out}), outflow mass and rate (M_{out} and \dot{M}_{out}), outflow momentum and its rate (p_{out} and \dot{p}_{out}), and total energy and its rate (E_{out} and \dot{E}_{out}). We also calculate the equivalent width ($\text{EW}_{\text{NaD, ISM}}$), a line quantity that also indicates the amount of outflowing mass. The assumptions used to infer these physical properties of outflows are the same as those adopted by the Blue Jay survey (Davies et al. 2024), which has also conducted a JWST/NIRSpec study of Na D outflows for a sample at cosmic noon. Specifically, the outflow velocity is defined as $v_{\text{out}} = |\Delta v| + 2\sigma$, where $\sigma = b/\sqrt{2}$ is the velocity dispersion of the ISM Na D line. For the outflow mass rate calculation, we use the relation:

$$\begin{aligned} \dot{M}_{\text{out}} &= \frac{M_{\text{out}} v_{\text{out}}}{r_{\text{out}}} \\ &= 11.45 \left(C_{\Omega} \frac{C_f}{0.4} \right) \left(\frac{N(\text{H I})}{10^{21} \text{ cm}^{-2}} \right) \\ &\quad \times \left(\frac{r_{\text{out}}}{1 \text{ kpc}} \right) \left(\frac{v_{\text{out}}}{200 \text{ km s}^{-1}} \right) M_{\odot} \text{ yr}^{-1}, \end{aligned}$$

where r_{out} is the outflow extent, C_{Ω} is the covering factor related to the wind opening angle, $N(\text{H I})$ is the hydrogen column density. We assume $r_{\text{out}} = 1 \text{ kpc}$ and $C_{\Omega} = 0.5$ as Davies et al. (2024) did. $N(\text{H I})$ is derived from $N(\text{Na I})$ assuming Milky-Way-like Na abundance and dust depletion factors and a 10% neutral fraction (see Rupke et al. 2005a), where $N(\text{Na I})$ is measured from the best-fit optical depth at the central ISM red Na D line $\tau_{r,0}$:

$$\begin{aligned} N(\text{Na I}) &= 10^{13} \left(\frac{\tau_{r,0}}{0.758} \right) \left(\frac{0.4164}{f_{lu}} \right) \\ &\quad \times \left(\frac{1215 \text{ \AA}}{\lambda_{lu}} \right) \left(\frac{b}{10 \text{ km s}^{-1}} \right) \text{ cm}^{-2}, \end{aligned}$$

where $f_{lu} = 0.32$ and $\lambda_{lu} = 5897.55 \text{ \AA}$ are the oscillator strength and rest-frame wavelength of the transition.

The uncertainty of \dot{M}_{out} derived from the MCMC fitting, i.e., random error, is only about ~ 0.1 dex, while its systematic errors coming from the assumptions of outflow structures and composition can be much larger. As Davies et al. (2024) discussed, C_{Ω} is unknown but cannot be smaller than 0.25 due to the outflow detection fraction in the Blue Jay survey, which can cause a factor of two difference in the inferred \dot{M}_{out} . Also, the neutral fraction of the outflow can range from 5% (Baron et al. 2020) to 10% (found by the Blue Jay survey), which could introduce another factor of two difference. Considering those two factors, the systematic uncertainty of the \dot{M}_{out} is about 0.6 dex. Furthermore, the radius of the outflow extent r_{out} is poorly constrained for Na D outflows at cosmic noon. However, given that the previous spatially-resolved outflow studies (e.g., Rupke & Veilleux 2015; Baron et al. 2020; D'Eugenio et al. 2024)

v_{out} (km s ⁻¹)	$\log(\text{N}(\text{Na I}))$ (cm ⁻²)	$\log(\text{N}(\text{H I}))$ (cm ⁻²)	$\log(M_{\text{out}})$ (M _⊙)	$\log(\dot{M}_{\text{out}})$ (M _⊙ yr ⁻¹)	$\log(p_{\text{out}})$	$\log(\dot{p}_{\text{out}})$	$\log(E_{\text{out}})$ (erg)	$\log(\dot{E}_{\text{out}})$ (erg s ⁻¹)
828 ⁺⁷⁹ ₋₄₉	14.39 ^{+0.13} _{-0.23}	22.03 ^{+0.13} _{-0.23}	8.47 ^{+0.12} _{-0.19}	2.40 ^{+0.11} _{-0.16}	49.69 ^{+0.11} _{-0.16}	36.11 ^{+0.11} _{-0.14}	57.30 ^{+0.11} _{-0.14}	43.73 ^{+0.11} _{-0.12}

Table 2. Neutral outflow properties of 216183.

suggest that 1 kpc is a lower limit of the size of Na D outflows which usually are even larger (a few to 15 kpc), our assumption would only result in the underestimation of \dot{M}_{out} that could even make JADES-GS-206183 more interesting than what we will state in Section 6.1.1.

After measuring the outflowing mass and mass outflow rate, we are then able to calculate the momentum and energy outflow rates. The final measurements of the outflow properties are listed in Table 2.

5.2. Comparison with Na D outflows in the literatures

In this section, we compare the properties of the Na D outflow in JADES-GS-206183 with Na D outflows detected in other galaxies at cosmic noon and in the local Universe.

At cosmic noon, the Blue Jay survey identified 14 Na D outflows (referred to as Blue Jay Na D outflows hereafter) at $z \sim 1.7\text{--}3.5$ using the NIRSpect MSA R ~ 1000 spectra (Davies et al. 2024). These outflows are found in galaxies spanning a range of types, from star-forming to quiescent, as well as both AGN-host and non-AGN host galaxies. The range of \dot{M}_{out} found for those Blue Jay Na D outflows is about $0.5\text{--}2 M_{\odot} \text{ yr}^{-1}$. Additionally, they found a decreasing trend in the mass loading factors ($\eta = \dot{M}_{\text{out}}/\text{SFR}$) of outflows with the SFRs of their host galaxies: the Na D outflows hosted by star-forming galaxies ($\text{SFR} > 10 M_{\odot} \text{ yr}^{-1}$) have a low mass loading factor ($\eta < 1$) while those in quiescent galaxies have $\eta > 1$. Interestingly, as shown in Figure 7, JADES-GS-206183 has a mass loading factor ~ 1 dex higher than the values of the Blue Jay outflows at this SFR range (typically around $\eta = 0$). The result indicates that the neutral outflow in JADES-GS-206183 is much more efficient in removing gas from the galaxy relative to the current formation of stars, compared to other observed Na D outflows launched in galaxies with comparable SFR.

We also compare the \dot{M}_{out} and \dot{E}_{out} of JADES-GS-206183 with Na D outflow measurements in the local Universe, including outflows found in Ultra Luminous Infrared Galaxies (ULIRGs) with AGN (Rupke et al. 2005b) and without AGN (Rupke et al. 2005c and Cazzoli et al. 2016), and post-starburst galaxies with AGN (Baron et al. 2022). As shown in Figure 8, the mass and energy loss through the Na D outflow in JADES-GS-206183 are comparable with the highest of the local

Na D outflows, rivaling those driven by intensive star forming or AGN activity.

5.3. AGN or not?

A natural explanation for exceptionally strong outflows is the presence of an AGN. In this section, we investigate the AGN activity in JADES-GS-206183 using different AGN diagnostics.

5.3.1. Archival multi-wavelength studies

First, we check whether JADES-GS-206183 has been classified as an AGN in the literature. In particular, we use the AGN catalogs from Lyu et al. (2022) and Lyu et al. (2024), which conducted one of the most comprehensive searches – using data from X-ray to radio, including the latest NIRC2 and MIRI data – for AGN populations at cosmic noon in GOODS-S. JADES-GS-206183 was not classified as an AGN host in these catalogs. In addition, JADES-GS-206183 has CO(2-1) and CO(5-4) observations from the ASPECS ALMA large program, which suggests that the CO excitation level of this galaxy is lower than that of AGN hosts, being more comparable to that of normal star-forming galaxies (Figure 5 in Boogaard et al. 2020), again, indicating JADES-GS-206183 does not host an on-going AGN.

5.3.2. Optical line ratio diagnostics

With our new NIRSpect/MSA observations, we can now investigate the AGN signatures (if any) in JADES-GS-206183 through its rest-optical spectral features. We first use the optical line ratio diagnostics, including the traditional [N II]-BPT diagram (Baldwin et al. 1981), and also [S II]- and [O I]-VO87 diagrams (Veilleux & Osterbrock 1987). As we mentioned in Section 3.1, the [O III] emission in JADES-GS-206183 is tentatively detected (1.5σ) (see Figure 1). Thus, we treat the [O III] flux as an upper limit. The BPT diagram is displayed in the left panel of Figure 9, where JADES-GS-206183 is located in the AGN-SF composite region between the boundaries defined by Kewley et al. (2001) and Kauffmann et al. (2003) at $z = 0$. Additionally, JADES-GS-206183 falls below the SF-AGN boundary at $z \sim 1.5$, as determined by Kewley et al. (2013). Thus, based on the BPT diagram, the ionization of JADES-GS-206183 is not consistent with an AGN.

The right two panels of Figure 9 also display the [S II]- and [O I]-VO87 diagrams. On the [S II]-VO87 diagram,

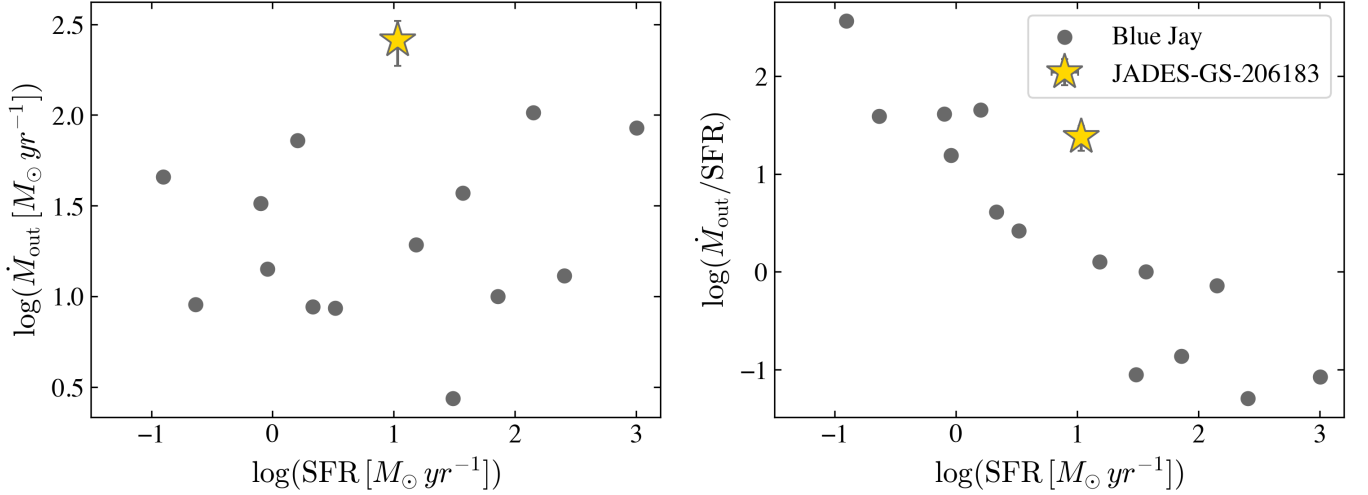


Figure 7. Comparison between JADES-GS-206183 (yellow stars) and the 14 Blue Jay $z \sim 2$ Na D outflows (Davies et al. 2024) (gray dots) in the SFR-mass outflow rate (left) and SFR-mass loading factor (right) planes. JADES-GS-206183’s Na D outflow exhibits a higher mass outflow rate and thus higher mass loading factor compared to the Na D outflows detected in the galaxies with similar SFR ($\log(\text{SFR}/M_{\odot} \text{ yr}^{-1}) \sim 1$) and redshift.

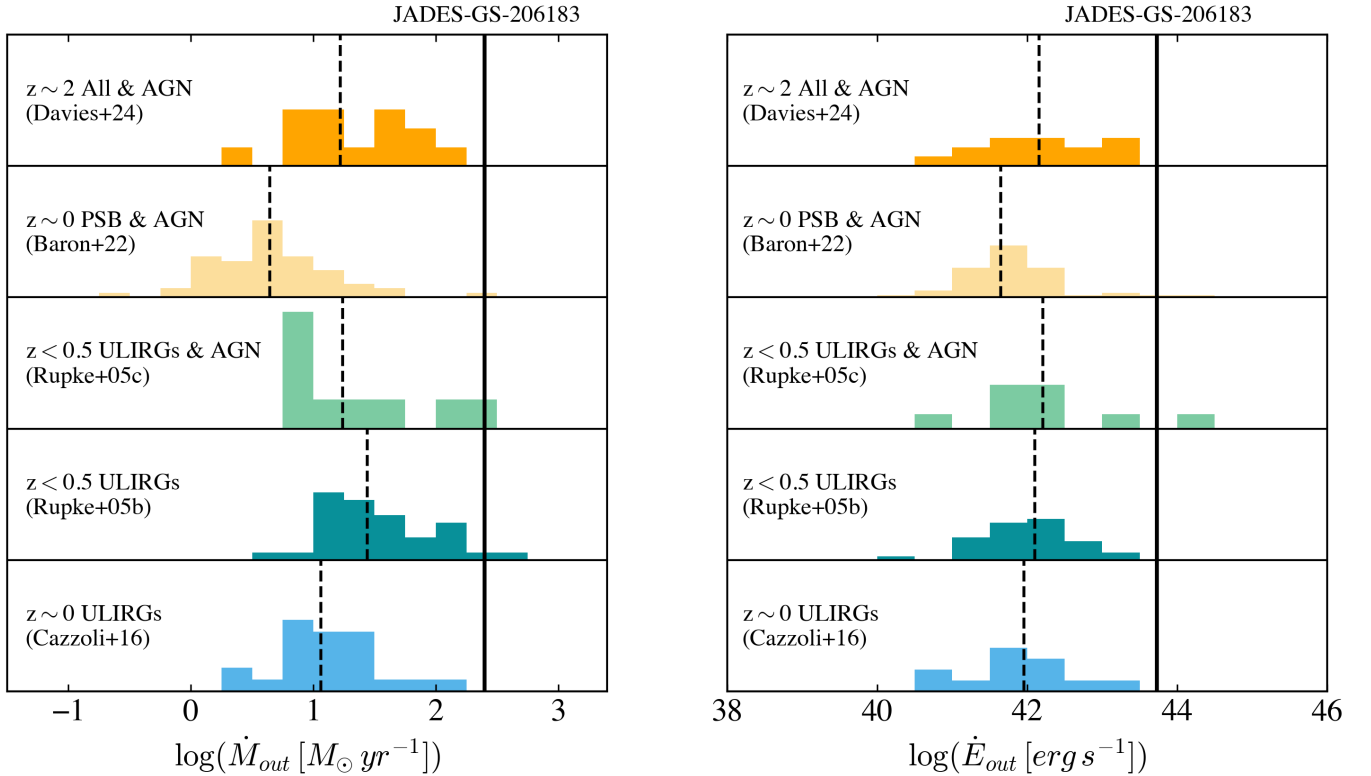


Figure 8. Comparison of neutral Na D outflow properties ($\log(\dot{M}_{\text{out}})$ on the left and $\log(\dot{E}_{\text{out}})$ on the right) in different samples, including 1) the outflows detected in the various types of $z \sim 2$ galaxies from the Blue Jay survey (Davies et al. 2024); 2) the local PSB AGN hosts from Baron et al. (2022); 3) the $z < 0.5$ Seyfert-2 ULIRGs from Rupke et al. (2005b); 4) the $z < 0.5$ SF/LINER ULIRGs from Rupke et al. (2005c); 5) the local pure-star forming ULIRGs from Cazzoli et al. (2016). The median values of each sample are shown by a black dashed line. The ($\log(\dot{M}_{\text{out}})$ and $\log(\dot{E}_{\text{out}})$ measurements of JADES-GS-206183 are illustrated by a solid line. Considering JADES-GS-206183 is an inactive PSB, the mass and energy outflow rate of its Na D outflow is surprisingly high compared to either the local or $z \sim 2$ outflows that are driven by powerful AGN or starbursts.

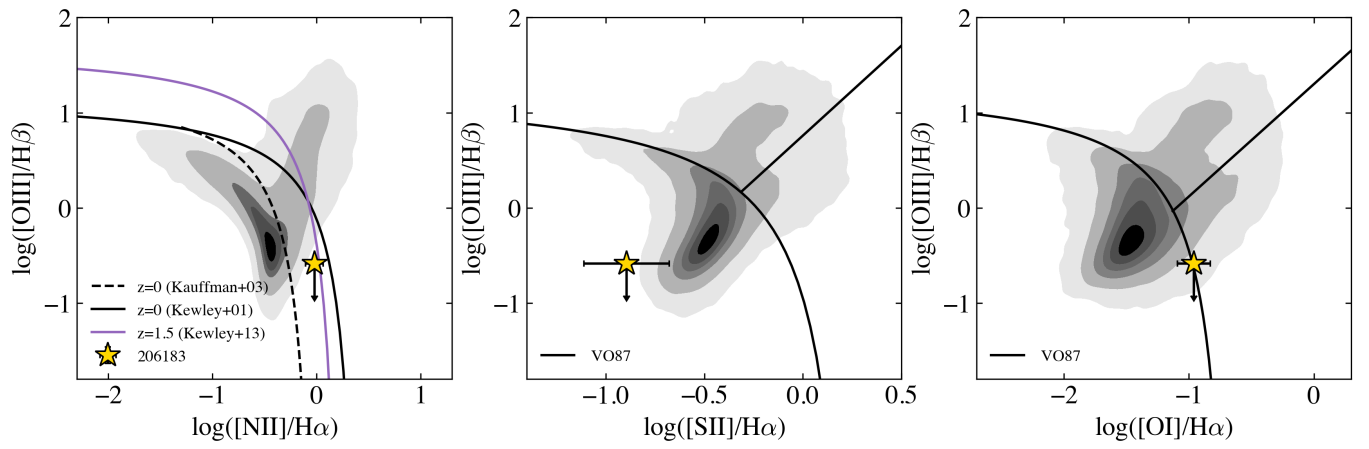


Figure 9. Location of JADES-GS-206183 (yellow stars) in the [N II]-BPT diagram (left), [S II]-VO87 diagram (middle), [O I]-VO87 diagram (right). The gray contours show the distribution of SDSS galaxies. The purple line in the left panel represents the redshift-dependent SF-AGN boundary at $z \sim 1.5$ determined by Kewley et al. (2013).

JADES-GS-206183 is sitting in the SF region, with a remarkably low $[\text{S II}]/\text{H}\alpha$ ratio. Given the low SNR of $[\text{S II}]$ in JADES-GS-206183, we caution that this abnormally low $[\text{S II}]/\text{H}\alpha$ ratio may be due to the uncertainty in the measurement of the $[\text{S II}]$ flux. On the $[\text{O I}]$ -version VO87 diagram, JADES-GS-206183 is just crossing the SF-LINER boundary.

To conclude, based on multiple AGN diagnostics using optical line ratios, there is no clear evidence for the presence of a strong AGN in JADES-GS-206183.

5.3.3. Broad $\text{H}\alpha$: AGN BLR or outflow?

As we mentioned in Section 3.1, our nebular emission line fitting suggests the presence of a broad component(s) to better fit the R \sim 1000 NIRSpect spectrum over the wavelength range covering $\text{H}\alpha$ and $[\text{N II}]$. If we assume this to be a single broad $\text{H}\alpha$ emission component, we obtain a line width of $\sim 2000 \text{ km s}^{-1}$. Such a line width is broadly consistent with what is usually observed in broad-line AGN. The brightness of this broad $\text{H}\alpha$ component would indicate an AGN with a bolometric luminosity of $\log(L_{\text{bol}}/\text{erg s}^{-1}) \sim 44.6$ using the bolometric corrections from Greene & Ho (2005); Netzer (2019). This corresponds to an X-ray Luminosity of $\log(L_{\text{X},2-10\text{keV}}/\text{erg s}^{-1}) \sim 43.5$ using the bolometric correction determined by Duras et al. (2020).

JADES-GS-206183 is close ($d \sim 4 \text{ arcmin}$) to the center of *Chandra* Deep Field South which has 7 Ms of deep X-ray imaging (Luo et al. 2017). With the broad- $\text{H}\alpha$ -inferred intrinsic X-ray luminosity, i.e. $\log(L_{\text{X},2-10\text{keV}}) \sim 43.5$, JADES-GS-206183 would have been detected in the *Chandra* imaging, unless it hosts a highly obscured SMBH with obscuration of $\log(N_{\text{H}}/\text{cm}^{-2}) \gtrsim 24$ (Figure 25 of Liu et al. 2017). Unfortunately, it is impossible for us to directly estimate obscuration towards JADES-GS-206183's central SMBH. Nonetheless, if we simply use the $A_V = 2.27$ from Hydrogen-line ratios (Section 3.3), we get a $\log(N_{\text{H}}/\text{cm}^{-2}) \sim 21.7$ using the A_V -to- N_{H} conversion of the Milky Way, which is orders of magnitude smaller than the obscuration inferred based on the non-detection of JADES-GS-206183 in X-ray. Although the levels of obscuration towards SMBH and averaged over the entire galaxy can differ significantly, this suggests that the broad $\text{H}\alpha$ component suggested by our previous line fitting may not originate from an AGN BLR.

More evidence against the AGN interpretation for the single, 2000 km s^{-1} -wide $\text{H}\alpha$ line comes from the analysis of the $\text{Pa}\alpha$ line profile observed in the FRESCO grism spectrum of JADES-GS-206183. To be specific, assuming the case B recombination and the AGN obscuration is comparable with that of the galactic ISM ($A_V = 2.27$),

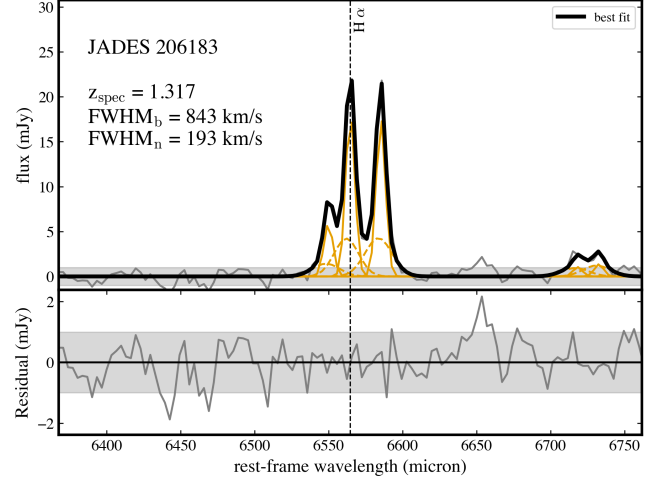


Figure 10. Line profile fitting for the $\text{H}\alpha$, $[\text{N II}]\lambda\lambda 6548, 6584$, and $[\text{S II}]\lambda\lambda 6717, 6731$, assuming the single broad component illustrated in the bottom right panel of Figure 1 is the superposition of three broad components originated from outflow. In the top panel, we show the stellar continuum subtracted 1D spectrum (gray line) and the best-fit line profile (black). The decomposed narrow components and broad components are plotted as the solid and dashed yellow lines, respectively. We show the residual and its 1σ level in the bottom panel.

we manually add a mock broad $\text{Pa}\alpha$ with the same velocity and dispersion as the broad $\text{H}\alpha$ component but a lower amplitude scaled from $\text{H}\alpha$. We confirm that our line fitting procedure should identify this broad $\text{Pa}\alpha$ component with $\Delta\text{BIC} > 10$. We also find, even in the most extreme case of $A_V = 0$, namely no dust attenuation towards the SMBH of JADES-GS-206183, we should still be able to detect the broad component in the $\text{Pa}\alpha$ line with $\Delta\text{BIC} > 10$. Therefore, the absence of clear evidence for a broad $\text{Pa}\alpha$ line in JADES-GS-206183's FRESCO grism spectrum strongly argues against the scenario of a single, 2000 km s^{-1} -wide broad $\text{H}\alpha$ line.

After considering all the aforementioned commonly used AGN diagnostics, we conclude that JADES-GS-206183 does not appear to host a strong AGN. This thus raises the question: what is the origin of the broad emission line component at the $\text{H}\alpha + [\text{N II}]$ wavelength range found in our spectral fitting? We note that the NIRSpect MSA spectroscopy for JADES-GS-206183 was conducted using medium-resolution gratings ($R \sim 1000$). At this spectral resolution, multiple broad emission components with moderately large widths can blend together, mimicking a single broad component with a much larger width. Thus, the broad emission line component could result from the superposition of three broad components, namely $\text{H}\alpha$ and the $[\text{N II}]$ doublet, generated by an ionized outflow.

To further test this scenario, we re-model the [N II]+H α line profile, as well as the nearby [S II] emission, using the “narrow+multi-broad” model on the stellar continuum-subtracted spectrum. The template contains a narrow and a broad component for [N II], H α , and [S II]. Again, for the narrow components, the velocity and its dispersion are fixed among all the lines. But for the broad components, we allow the line width and offset of the broad H α to be different from the width of [N II] and [S II], accounting for additional AGN contribution to the H α line besides outflows. In addition, we require all of the broad components to be wider than 500 km s⁻¹. The best-fit H α profile is shown in Figure 10. The resulting FWHM of the narrow component, broad H α component, and broad [N II](or [S II]) component are 193 ± 35 , 843 ± 154 , and 940 ± 169 km s⁻¹, respectively. This indicates that the broad components of H α , [N II], and [S II] have the same width within the measurement uncertainties. Also, all of the broad components are consistent with systemic velocity considering the spectral resolution (see Table 1). Therefore, the best-fit “narrow+multi-broad” model suggests the broad component of H α , [N II], and [S II] should trace the same gas kinematics, which is consistent with the outflow-only scenario, without additional AGN BLR emission. Also, we find that the BIC of the multiple broad [N II]+H α model is comparable with that of the single broad H α model used in Section 3.1 ($\Delta BIC < 5$), suggesting that the model representing the outflow scenario can produce a similarly good fit for the data compared to the AGN BLR model.

In addition, we also test whether we could detect a similarly outflow-broadened Pa α component, as we did for a single broad H α scenario. The result turns out that, if the outflowing materials in JADES-GS-206183 experience the same attenuation as the galaxy ISM ($A_V = 2.27$), then we would also be able to detect a broad Pa α component. However, a systematic study of outflows in local ULIRGs (Fluetsch et al. 2021) suggests that the A_V of outflowing gas is typically one magnitude lower than the global attenuation. In this case, if assuming the A_V for the outflow is 1.27 magnitude, we would not have a robust detection of the Pa α broad component resulting from the outflow ($\Delta BIC < 10$). While the attenuation level of the outflow in quenching galaxies at $z > 1$ may differ from those in local ULIRGs, this test could suggest that the ionized outflowing gas in JADES-GS-206183 has lower attenuation than the systemic ISM.

In conclusion, we do not find strong evidence for AGN presence in JADES-GS-206183. The broad (~ 2000 km s⁻¹) H α component suggested by our initial

spectral fitting is most likely the result of three moderately broad (~ 900 km s⁻¹) lines—[N II] doublet and H α —blended together due to the limited spectral resolution, which is consistent with expectations for an outflow. Thus, we argue that the origin of these broad lines is more consistent with ionized outflows, rather than AGN. Finally, we reported the measured fluxes of [N II], H α , and [S II] based on the “outflow” model, as well as the bootstrap-derived uncertainties in Table 1.

6. DISCUSSION

6.1. Outflow Driving Mechanism

As highlighted in Section 5.2, the Na D outflow in JADES-GS-206183 is among the most powerful and energetic neutral outflows known at $z < 3$. This naturally raises the questions: *Why is this neutral outflow so powerful? what is driving such a strong outflow in this galaxy?*

6.1.1. Current SF or AGN?

Star formation and AGN are the two sources that can power strong galactic outflow (King & Pounds 2015; Rupke 2018). In the local universe, Na D outflow is commonly detected in star-forming systems (e.g., Rupke et al. 2005c; Chen et al. 2010; Concas et al. 2019), especially starburst galaxies and ULIRGs. Meanwhile, many works have found that the local Na D outflow strength and incidence are independent of the level of nuclear activity, suggesting that the physical mechanisms driving neutral gas outflows may be more closely related to galaxy star formation than to AGN activity in star-forming galaxies. However, Na D outflows are also detected in local PSBs (e.g., Baron et al. 2022; Sun et al. 2024) – whose star formation has been quickly shut down in the past 1 Gyr – indicating that neutral outflows found in these systems cannot be powered by their *instantaneous* star formation. For PSBs hosting AGNs (e.g., Baron et al. 2022), the neutral outflows are therefore naturally attributed to AGN activity, particularly through AGN-driven galactic winds.

At cosmic noon, a consensus on neutral gas outflows, particularly regarding their driving mechanisms, has yet to be reached. The 14 Na D outflows recently identified by the Blue Jay survey (Davies et al. 2024) are more likely driven by AGNs, given that the majority of these outflows are found in galaxies with low SFRs, which cannot account for the strengths of the outflows inferred from their Na D features. Belli et al. (2024) studied one of those Na D outflows detected in a PSB at $z \sim 2.5$ in detail, finding its host exhibits AGN signatures through the BPT line-ratio diagnostics. In addition, D’Eugenio et al. (2024) also detected a multiphase outflow (includ-

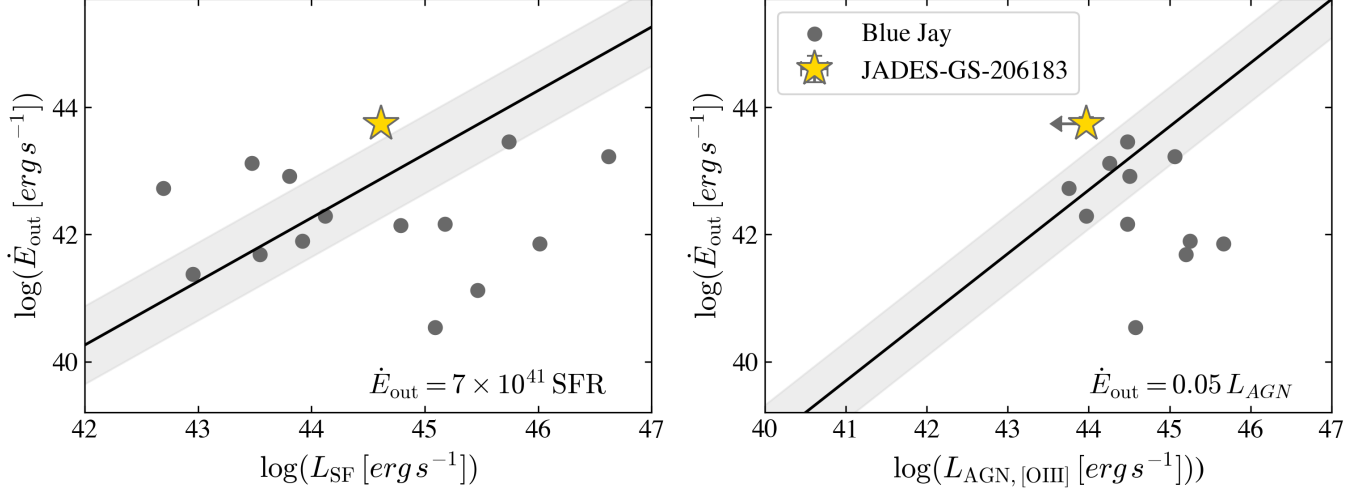


Figure 11. Energy outflow rate of JADES-GS-206183 (yellow stars) compared to the luminosity from SF (left) and AGN (right). Given the non-detection of $[\text{O III}]\lambda 5007$, we estimate an upper limit of $[\text{O III}]$ -derived AGN luminosity based on the flux uncertainty. For comparison, the Blue Jay Na D outflows are also shown in the figures by gray dots. The black solid lines represent the expected outflow kinetic energy driven by star formation or AGN. The surrounding shaded regions are the typical uncertainties of outflow energy rate measurement brought by the assumptions of outflow opening angle and covering fraction (see Section 5.1).

ing Na D-traced neutral phase) at a $z \sim 3$ PSB which also has ongoing AGN activities.

As we discussed above (Section 4 and 3.3), JADES-GS-206183 is a quenching galaxy with low current star formation. In addition, its central BH seems not to be actively accreting (Section 5.3). Those findings seem to question the scenario that current intense activity powers the outflow.

To quantitatively understand whether instantaneous star formation or AGN could drive the neutral outflow in JADES-GS-206183, we follow Davies et al. (2024) to estimate the energies that could be provided by these mechanisms and compare them with the kinetic energy of the Na D outflow. We first calculate the star formation luminosity of JADES-GS-206183 as $L_{\text{SF}} \approx \text{SFR}_{\text{Pa}\alpha} \times 10^{10} L_{\odot}$ (erg s^{-1}). We also estimate the AGN luminosity using the $[\text{O III}]$ bolometric correction by Netzer (2009) ($L_{\text{bol}} = 600 L_{[\text{O III}]}$ erg s^{-1}). However, we note that the $[\text{O III}]$ -derived AGN bolometric luminosity is problematic because $L_{[\text{O III}]}$ of an AGN is sensitive to the physical state of the AGN BLR and obscuration (Diamond-Stanic et al. 2009; Pennell et al. 2017; Netzer 2019). Moreover, as we mentioned in Section 5.3, the $[\text{O III}]$ emission is actually not detected for which we derive just a flux upper limit. Taking those caveats, we obtain the $[\text{O III}]$ -derived AGN luminosity upper limit with $\log(L_{\text{bol}}/\text{erg s}^{-1}) < 43.97$.

Figure 11 displays the comparison between the energy rate of the Na D outflows and the star formation and AGN luminosities, for both JADES-GS-206183

and the Blue Jay outflows. We overplot two reference lines – based on theoretical models – of the maximum energy rate that could be provided by star formation and AGN. If we assume that supernovae are the main energy source of a star formation-driven outflow, the mechanical energy rate they could provide is $\dot{E}_{\text{SN}}(\text{erg s}^{-1}) = 7 \times 10^{41} \text{SFR}(\text{M}_{\odot} \text{yr}^{-1})$, the relation from Veilleux et al. (2005) based on solar metallicity Starburst99 models (Leitherer et al. 1999). For an AGN-driven outflow, King & Pounds (2015) found that 5% of the AGN bolometric luminosity could be transferred to the outflow kinetic energy in the energy-conserving scenario.

Unlike the strengths of the Blue Jay outflows which can all be explained by either SF or AGN, for JADES-GS-206183, we find that its observed outflow energy rate is about 1 dex higher than both the SN-powered outflow energy rate given its current SFR, and the expected AGN-driven outflow energy rate considering its $[\text{O III}]$ -derived AGN luminosity. Moreover, the combination of the SN+AGN energy budget is still not sufficient to drive the observed outflow. That is, neither ongoing star formation nor nuclear activity could power the strong Na D outflow in JADES-GS-206183. This result will be even more robust if:

1. the extent of the JADES-GS-206183 outflow is larger than 1 kpc in radius, the value we conservatively assume, a possibility supported by the observations of other Na D outflows that can extend to ~ 10 kpc;

2. the true AGN bolometric luminosity of JADES-GS-206183 is lower than the upper limit estimation derived from the [O III] flux upper limit.

6.1.2. Fossil Outflow?

Since neither instantaneous star formation nor AGN activity appears to be sufficiently powerful to produce the strengths of the neutral outflow observed in JADES-GS-206183, we now explore another possible mechanism: a fossil outflow powered by previous intense starbursts and/or AGN activity. This process has been proposed to explain some neutral outflows found in nearby PSBs (Sun et al. 2024).

The dynamical timescale of the observed outflow can be estimated as $t_{dyn} = r_{out}/v_{out}$. Considering r_{out} is 1 kpc, and its current outflow velocity is about 800 km s^{-1} , the t_{dyn} of the Na D outflow in JADES-GS-206183 is about 2 Myr, which can reach to ~ 10 Myr if considering a much larger r_{out} . Therefore, to test this fossil outflow scenario, from this point on, we will be focusing on estimating the star formation and AGN activities over the past 10 Myr in JADES-GS-206183.

We can assume JADES-GS-206183 retains the low star formation rate derived in Section 3.3 for the past 10 Myr ($\text{SFR}_{Pa\alpha} \sim 10 M_{\odot} \text{ yr}^{-1}$). Therefore, the accumulated energy injected by star formation in the past 10 Myr is still not sufficient to drive the neutral outflow we observed.

On the other hand, the dynamical timescale of the Na D outflows in JADES-GS-206183 is a little shorter than but overall comparable to the typical long-term AGN activity phase duration, which is about 10 Myr (Hopkins et al. 2005). Within each phase, numerous individual episodes with durations $\sim 0.1 \text{ Myr}$ may occur (e.g., Hickox et al. 2014). As a consequence, it is likely that the outflow could persist within the galaxy after an AGN has switched off. Moreover, we would expect multiple AGN energy injections to occur during the expansion of the outflow, which could continuously power the outflow (Zubovas & Nardini 2020) and affect its dynamical and thermal equilibrium. Interestingly, Zubovas et al. (2022) adopted a neural network to analyze AGN luminosity histories in 59 observed AGN-driven molecular outflows and found that the average AGN duty cycle in those outflow systems is $\delta_{AGN} \sim 0.6$. The result from Zubovas et al. (2022) suggests that more than half of the AGN-driven outflows may be detected in inactive galaxies whose AGN have shut down.

In addition, JADES-GS-206183 has a clear bar structure and two spiral arms shown in its NIRCам F115W/F200W/F356W RGB image (Figure 1). Bar-driven processes are often considered as an efficient tun-

nel to drive gas to the center of the galaxy, feeding the BH accretion and thus lighting it up as an AGN. Many observational works have confirmed the bar-AGN connection through the correlation between the AGN luminosity and bar strength, as well as the higher AGN incidence in barred galaxies (Silva-Lima et al. 2022 and references therein). In terms of this, the well-constructed bar shown in JADES-GS-206183 could also indicate that, maybe at some point before, its bar was able to transport a lot of gas into the nuclear region to trigger the AGN activity, but later on, the tunnel had been shut down, given that we do not observe any ongoing AGN nowadays.

We estimate whether JADES-GS-206183 could have a powerful enough AGN to launch outflows in the past by estimating its central black hole mass (M_{\bullet}) and the inferred Eddington luminosity using the stellar mass derived through SED fitting (Section 4). Adopting the M_{\bullet} - M_{*} relation at $1 < z < 4$ ($\log(M_{\bullet}/M_{*}) = -2.5$) from Sun et al. (2025), we obtain an M_{\bullet} of JADES-GS-206183 of $\sim 10^{8.5} M_{\odot}$, corresponding to an Eddington luminosity of $\sim 5 \times 10^{46} \text{ erg s}^{-1}$. This means that past AGN activity in JADES-GS-206183 could easily drive the strong outflows we observe now: the observed outflow energy rate $\dot{E}_{out} \sim 0.05 L_{bol}$ can be achieved once its Eddington ratio ($\lambda_{Edd} = L_{bol}/L_{Edd}$) is higher than 0.02.

Our study can be put into a broader context through the work of Taylor et al. (2024), who stacked the Mg II spectra of 264 galaxies from the UKIRT Ultra-Deep Survey (UDS) to search for the neutral outflows at $z > 1$. They found that high-velocity outflows were not found in galaxies whose star formation has shut down > 1 Gyr ago, but that outflow velocities similar to that in JADES-GS-206183 did occur in their two samples with star formation of age < 0.6 Gyr and between 0.6 and 1 Gyr. This presented them with a similar dilemma to the one we face: (1) contrary to the high outflow velocities, Sun et al. (2024) have shown that outflow velocities decrease with time from an energetic episode of star formation; and (2) if driven by star formation, the very high mass loading factor for JADES-GS-206183 reflects a high past energy input to the outflow coupled with a small current SFR, but as a stellar population ages, the energy input into outflows (e.g., type II supernovae) decreases. Taylor et al. (2024) conclude, as we do, that the outflows in their sample are likely to be powered by episodic AGN activity.

6.1.3. What makes JADES-GS-206183's outflow exceptionally strong?

In addition, the hypothesis of a fossil AGN-driven outflow may also explain why the Na D outflow in JADES-

GS-206183 is so powerful, even comparable with those in local ULIRGs with ongoing AGN activities. If we are seeing an AGN-driven outflow that has been powered by multiple individual AGN episodes during the whole long-term AGN activity phase that has now died out, or where we are between outbursts, then we may have caught this system at a special time. In that case, it would not be surprising that this Na D outflow is the strongest one known at cosmic noon, given the modest numbers observed to date at $z > 1$. On the contrary, in the local Universe, Sun et al. (2024) has discovered a much larger number (~ 100) of Na D outflows in PSBs without strong ongoing AGN activities, among which some do have a comparably high outflow velocity as JADES-GS-206183. Therefore, those local Na D outflows might also be witnessed by us at a similar time point as JADES-GS-206183 – the end of the long-term AGN phase. Those outflows observed at such a unique time are essential for understanding the detailed mechanism of episodic-AGN-driven outflow, especially its time evolution.

6.2. Multiphase outflow

Galactic outflows are commonly multiphase. In JADES-GS-206183, besides the neutral outflow traced by Na D absorption, we also find tentative evidence of an ionized-phase outflow.

In Section 5.3, we have shown that the profile of [N II], H α , and [S II] of JADES-GS-206183 suggest they may share the same broad component, which is consistent with expectations of a warm ionized outflow. However, due to the limited spectral resolution and the complexity of the [N II]+H α profile, the kinematics of ionizing gas derived from multiple component fitting would be uncertain. Therefore, we do not quantify the ionized outflow properties in this work.

Another tentative indication for an ionized outflow is that, from the MUSE IFS data, we mapped the [O II] $\lambda\lambda 3726, 3729$ emission of this galaxy. Even though the seeing of $\sim 0.8''$ does not enable us to construct a meaningful velocity and velocity dispersion map of [O II] emission, the whole [O II] flux map provides useful information on galactic-scale ionized gas distribution. The left panel of Figure 5 shows that, this emission is extended to the upper left region up to $\sim 1''$ relative to the galaxy stellar distribution. This [O II] extension is consistent with the position of the strong Na D outflow. The MSA shutter was oriented from the upper left to the lower right and the center is slightly shifted to the upper left. Therefore, the Na D outflow we observed from the SMILES NIRSpec MSA spectrum should come from the upper left region of JADES-GS-

206183's center. Therefore, we speculate that the extended [O II] emission may trace the ionized outflowing gas coupled with the Na D-traced neutral outflow. A future higher spatial-resolution IFU observation of ionized outflow tracers is crucial to confirm the existence of any ionized-phase outflow and its spatial distribution.

7. CONCLUSION

In this work, using the new JWST NIRSpec/MSA spectrum collected by the SMILES survey, we identified an extremely strong neutral outflow traced by Na D $\lambda\lambda 5890, 5896$ in the inactive quenching galaxy JADES-GS-206183 at $z = 1.317$. Our main findings are the following:

- By subtracting the stellar continuum modelled by pPXF from the whole NIRSpec spectrum, we uncovered a significantly deep and blueshifted Na D ISM absorption (Figure 1), corresponding to a powerful outflow with a velocity of $v_{\text{out}} = 828_{-49}^{+79} \text{ km s}^{-1}$, a mass outflow rate of $\log(\dot{M}_{\text{out}}/\text{M}_{\odot} \text{ yr}^{-1}) = 2.40_{-0.16}^{+0.11}$, and an energy outflow rate of $\log(\dot{E}_{\text{out}}/\text{erg s}^{-1}) = 43.73_{-0.12}^{+0.11}$.
- Comparing the outflow properties of JADES-GS-206183 with the Na D outflows at cosmic noon identified by the Blue Jay survey from Davies et al. (2024), as well as the outflows in the local ULIRGs and PSBs with/without AGNs, we found the JADES-GS-206183 Na D outflow has the highest mass outflow rate at $z > 1$ (Figure 7), also at the top of the Na D outflows in the local galaxies with ongoing intensive SF/AGN activities (Figure 8).
- From the SED reconstructed from photometries in 22 bands from HST/ACS and WFC3 to JWST/NIRCam, we derived the stellar mass of $\log(M_*/\text{M}_{\odot}) = 11.15_{-0.05}^{+0.04}$ and SFH for JADES-GS-206183. The SED fitting results suggest that JADES-GS-206183 is a massive quiescent/post-starburst galaxy in which star formation has ceased in the past 1 Gyr (Figure 6). The quiescent nature is also supported by its prominent stellar absorption features revealed by the SMILES NIRSpec data. In addition, we measured the Pa α emission captured by the FRESCO NIRCam grism spectrum to derive an accurate current SFR of $10.78 \pm 0.55 \text{ M}_{\odot} \text{ yr}^{-1}$, consistent with the SED-derived value, again confirming that JADES-GS-206183 has a low level of star formation.
- We measured the fluxes of the four BPT emission lines H β , H α , [O III], and [N II] from the SMILES

NIRSpec spectrum and determined the locus of JADES-GS-206183 in the BPT and VO87 diagrams. JADES-GS-206183 has just a tentative detection of [O III] (Figure 1), which only allows us to derive an upper limit on the [O III] flux. JADES-GS-206183 is located in the composite area (Figure 9), and also in the non-AGN region in VO87 diagrams. Moreover, the detected broad component of H α is more likely to originate from an ionized outflow, rather than an AGN BLR (Figure 10). Along with its non-AGN classification from Lyu et al. (2022, 2024), JADES-GS-206183 seems not to host a strong AGN.

- The current weak star formation and AGN activity ($\log(L_{bol,[O\ III]}/\text{erg s}^{-1}) < 43.97$) in JADES-GS-206183 are not sufficient to power the observed strong Na D outflow. In Figure 11, this result was confirmed by comparing the observed energy rate of JADES-GS-206183 with the theoretical values considering the energy injection from current star formation and AGN (as a function of SFR and L_{bol}). Therefore, we speculate that the strong Na D outflow we observed in JADES-GS-206183 might be an AGN-driven fossil outflow. As a consequence, the fact that this outflow is extremely strong could then be explained by the scenario that we might be witnessing this outflow at a unique time – the end of a long-term AGN activity phase, in which the outflow has been episodically powered and speeded up by multiple AGN activities during the whole phase.
- From the MUSE IFS observations of JADES-GS-206183, we built the [O II] emission map (Figure 5) and found it seems to extend to the same direction as the Na D outflow (constrained by the position of the MSA shutter). Along with the outflow interpretation of the broad component detected in H α , the results suggest the outflow in JADES-GS-206183 might be multiphase.

To fully confirm the exact wind-driving mechanism, and understand the timescale of energy source and outflow evolution, it is crucial to obtain the spatially-resolved spectroscopic (e.g. NIRSpec/IFU) observation, which will be essential to map the outflow extent, as well as the spatial distribution of the physical properties of the outflowing gas, such as velocity, mass, temperature. Meanwhile, IFU observations will enable us to map the host galaxy properties, which will reveal the AGN and outflow impact on the host star formation activities, helping us link the outflow to the quenching

process in JADES-GS-206183. Finally, along with other multi-wavelength data, e.g., ALMA high-resolution observations are necessary to build a more comprehensive picture of the multiphase outflow of this galaxy.

8. ACKNOWLEDGMENTS

YS, ZJ, YZ, and CNAW acknowledge support from the NIRCам Science Team contract to the University of Arizona, NAS5-02015. GHR acknowledges support from the JWST Mid-Infrared Instrument (MIRI) Science Team Lead, grant 80NSSC18K0555, from NASA Goddard Space Flight Center to the University of Arizona. FDE acknowledges support by the Science and Technology Facilities Council (STFC), by the ERC through Advanced Grant 695671 “QUENCH”, and by the UKRI Frontier Research grant RISEandFALL. AJB acknowledges funding from the “FirstGalaxies” Advanced Grant from the European Research Council (ERC) under the European Union’s Horizon 2020 research and innovation programme (Grant agreement No. 789056).

This work is based on observations made with the VLT/ MUSE and the NASA/ESA/CSA James Webb Space Telescope. MUSE observations used in this work are taken by the MUSE Hubble UDF Survey as parts of the MUSE Consortium, for which the data can be accessed via the AMUSED website <https://amused.univ-lyon1.fr/project/UDF/>. The JWST data were obtained from the Mikulski Archive for Space Telescopes at the Space Telescope Science Institute, which is operated by the Association of Universities for Research in Astronomy, Inc., under NASA contract NAS 5-03127 for JWST. These observations are associated with programs 1180, 1207, and 1895, for which the data can be accessed via <https://doi.org/10.17909/8tdj-8n28> (Rieke et al. 2023a), <https://doi.org/10.17909/et3f-zd57> (Rieke, George et al. 2024), and <https://doi.org/10.17909/gdyc-7g80> (Oesch & Magee 2023).

We respectfully acknowledge the University of Arizona is on the land and territories of Indigenous peoples. Today, Arizona is home to 22 federally recognized tribes, with Tucson being home to the O’odham and the Yaqui. The University strives to build sustainable relationships with sovereign Native Nations and Indigenous communities through education offerings, partnerships, and community service.

Facilities: JWST, VLT/MUSE

Software: `AstroPy` (Astropy Collaboration et al. 2013, 2018, 2022), `emcee` (Foreman-Mackey et al. 2013b), `lmfit` (Newville et al. 2014), `mpdaf` (Bacon et al. 2016), `Prospector` (Johnson et al. 2021), `SciPy` (Virtanen et al. 2020)

REFERENCES

- Alberts, S., Lyu, J., Shivaee, I., et al. 2024, *ApJ*, 976, 224, doi: [10.3847/1538-4357/ad7396](https://doi.org/10.3847/1538-4357/ad7396)
- Astropy Collaboration, Robitaille, T. P., Tollerud, E. J., et al. 2013, *A&A*, 558, A33, doi: [10.1051/0004-6361/201322068](https://doi.org/10.1051/0004-6361/201322068)
- Astropy Collaboration, Price-Whelan, A. M., Sipőcz, B. M., et al. 2018, *AJ*, 156, 123, doi: [10.3847/1538-3881/aabc4f](https://doi.org/10.3847/1538-3881/aabc4f)
- Astropy Collaboration, Price-Whelan, A. M., Lim, P. L., et al. 2022, *ApJ*, 935, 167, doi: [10.3847/1538-4357/ac7c74](https://doi.org/10.3847/1538-4357/ac7c74)
- Bacon, R., Piqueras, L., Conseil, S., Richard, J., & Shepherd, M. 2016, MPDAF: MUSE Python Data Analysis Framework, Astrophysics Source Code Library, record ascl:1611.003
- Bacon, R., Brinchmann, J., Conseil, S., et al. 2023, *A&A*, 670, A4, doi: [10.1051/0004-6361/202244187](https://doi.org/10.1051/0004-6361/202244187)
- Baldwin, J. A., Phillips, M. M., & Terlevich, R. 1981, *PASP*, 93, 5, doi: [10.1086/130766](https://doi.org/10.1086/130766)
- Baron, D., & Netzer, H. 2019, *MNRAS*, 486, 4290, doi: [10.1093/mnras/stz1070](https://doi.org/10.1093/mnras/stz1070)
- Baron, D., Netzer, H., Davies, R. I., & Xavier Prochaska, J. 2020, *MNRAS*, 494, 5396, doi: [10.1093/mnras/staa1018](https://doi.org/10.1093/mnras/staa1018)
- Baron, D., Netzer, H., Lutz, D., Prochaska, J. X., & Davies, R. I. 2022, *MNRAS*, 509, 4457, doi: [10.1093/mnras/stab3232](https://doi.org/10.1093/mnras/stab3232)
- Belli, S., Park, M., Davies, R. L., et al. 2024, *Nature*, 630, 54, doi: [10.1038/s41586-024-07412-1](https://doi.org/10.1038/s41586-024-07412-1)
- Boogaard, L. A., Decarli, R., González-López, J., et al. 2019, *ApJ*, 882, 140, doi: [10.3847/1538-4357/ab3102](https://doi.org/10.3847/1538-4357/ab3102)
- Boogaard, L. A., van der Werf, P., Weiss, A., et al. 2020, *ApJ*, 902, 109, doi: [10.3847/1538-4357/abb82f](https://doi.org/10.3847/1538-4357/abb82f)
- Bushouse, H., Eisenhamer, J., Dencheva, N., et al. 2022, JWST Calibration Pipeline, 1.6.2, Zenodo, doi: [10.5281/zenodo.7041998](https://doi.org/10.5281/zenodo.7041998)
- Bushouse, H., Eisenhamer, J., Dencheva, N., et al. 2024, JWST Calibration Pipeline, Zenodo, doi: [10.5281/ZENODO.6984365](https://doi.org/10.5281/ZENODO.6984365)
- Byler, N., Dalcanton, J. J., Conroy, C., & Johnson, B. D. 2017, *ApJ*, 840, 44, doi: [10.3847/1538-4357/aa6c66](https://doi.org/10.3847/1538-4357/aa6c66)
- Calzetti, D., Armus, L., Bohlin, R. C., et al. 2000, *ApJ*, 533, 682, doi: [10.1086/308692](https://doi.org/10.1086/308692)
- Cappellari, M. 2017, *MNRAS*, 466, 798, doi: [10.1093/mnras/stw3020](https://doi.org/10.1093/mnras/stw3020)
- Cappellari, M. 2023, *MNRAS*, 526, 3273, doi: [10.1093/mnras/stad2597](https://doi.org/10.1093/mnras/stad2597)
- Cappellari, M., & Emsellem, E. 2004, *PASP*, 116, 138, doi: [10.1086/381875](https://doi.org/10.1086/381875)
- Carnall, A. C., McLure, R. J., Dunlop, J. S., et al. 2023, *Nature*, 619, 716, doi: [10.1038/s41586-023-06158-6](https://doi.org/10.1038/s41586-023-06158-6)
- Carniani, S., Venturi, G., Parlanti, E., et al. 2024, *A&A*, 685, A99, doi: [10.1051/0004-6361/202347230](https://doi.org/10.1051/0004-6361/202347230)
- Cazzoli, S., Arribas, S., Maiolino, R., & Colina, L. 2016, *A&A*, 590, A125, doi: [10.1051/0004-6361/201526788](https://doi.org/10.1051/0004-6361/201526788)
- Chabrier, G. 2003, *PASP*, 115, 763, doi: [10.1086/376392](https://doi.org/10.1086/376392)
- Chen, Y.-M., Tremonti, C. A., Heckman, T. M., et al. 2010, *AJ*, 140, 445, doi: [10.1088/0004-6256/140/2/445](https://doi.org/10.1088/0004-6256/140/2/445)
- Choi, J., Dotter, A., Conroy, C., et al. 2016, *ApJ*, 823, 102, doi: [10.3847/0004-637X/823/2/102](https://doi.org/10.3847/0004-637X/823/2/102)
- Cicone, C., Maiolino, R., Sturm, E., et al. 2014, *A&A*, 562, A21, doi: [10.1051/0004-6361/201322464](https://doi.org/10.1051/0004-6361/201322464)
- Coil, A. L., Weiner, B. J., Holz, D. E., et al. 2011, *ApJ*, 743, 46, doi: [10.1088/0004-637X/743/1/46](https://doi.org/10.1088/0004-637X/743/1/46)
- Concas, A., Popesso, P., Brusa, M., Mainieri, V., & Thomas, D. 2019, *A&A*, 622, A188, doi: [10.1051/0004-6361/201732152](https://doi.org/10.1051/0004-6361/201732152)
- Conroy, C., & Gunn, J. E. 2010, *ApJ*, 712, 833, doi: [10.1088/0004-637X/712/2/833](https://doi.org/10.1088/0004-637X/712/2/833)
- Conroy, C., Gunn, J. E., & White, M. 2009, *ApJ*, 699, 486, doi: [10.1088/0004-637X/699/1/486](https://doi.org/10.1088/0004-637X/699/1/486)
- Couch, W. J., & Sharples, R. M. 1987, *MNRAS*, 229, 423, doi: [10.1093/mnras/229.3.423](https://doi.org/10.1093/mnras/229.3.423)
- Davies, R., Baron, D., Shimizu, T., et al. 2020, *MNRAS*, 498, 4150, doi: [10.1093/mnras/staa2413](https://doi.org/10.1093/mnras/staa2413)
- Davies, R. L., Belli, S., Park, M., et al. 2024, *MNRAS*, 528, 4976, doi: [10.1093/mnras/stae327](https://doi.org/10.1093/mnras/stae327)
- de Graaff, A., Setton, D. J., Brammer, G., et al. 2024, *Nature Astronomy*, doi: [10.1038/s41550-024-02424-3](https://doi.org/10.1038/s41550-024-02424-3)
- D'Eugenio, F., Pérez-González, P. G., Maiolino, R., et al. 2024, *Nature Astronomy*, 8, 1443, doi: [10.1038/s41550-024-02345-1](https://doi.org/10.1038/s41550-024-02345-1)
- D'Eugenio, F., Cameron, A. J., Scholtz, J., et al. 2025, *ApJS*, 277, 4, doi: [10.3847/1538-4365/ada148](https://doi.org/10.3847/1538-4365/ada148)
- Diamond-Stanic, A. M., Rieke, G. H., & Rigby, J. R. 2009, *ApJ*, 698, 623, doi: [10.1088/0004-637X/698/1/623](https://doi.org/10.1088/0004-637X/698/1/623)
- Dressler, A., & Gunn, J. E. 1983, *ApJ*, 270, 7, doi: [10.1086/161093](https://doi.org/10.1086/161093)
- Duras, F., Bongiorno, A., Ricci, F., et al. 2020, *A&A*, 636, A73, doi: [10.1051/0004-6361/201936817](https://doi.org/10.1051/0004-6361/201936817)
- Eisenstein, D. J., Willott, C., Alberts, S., et al. 2023a, *arXiv e-prints*, arXiv:2306.02465, doi: [10.48550/arXiv.2306.02465](https://doi.org/10.48550/arXiv.2306.02465)
- Eisenstein, D. J., Johnson, B. D., Robertson, B., et al. 2023b, *arXiv e-prints*, arXiv:2310.12340, doi: [10.48550/arXiv.2310.12340](https://doi.org/10.48550/arXiv.2310.12340)
- Falcón-Barroso, J., Sánchez-Blázquez, P., Vazdekis, A., et al. 2011, *A&A*, 532, A95, doi: [10.1051/0004-6361/201116842](https://doi.org/10.1051/0004-6361/201116842)

- Ferruit, P., Jakobsen, P., Giardino, G., et al. 2022, A&A, 661, A81, doi: [10.1051/0004-6361/202142673](https://doi.org/10.1051/0004-6361/202142673)
- Feruglio, C., Fiore, F., Carniani, S., et al. 2015, A&A, 583, A99, doi: [10.1051/0004-6361/201526020](https://doi.org/10.1051/0004-6361/201526020)
- Fluetsch, A., Maiolino, R., Carniani, S., et al. 2021, MNRAS, 505, 5753, doi: [10.1093/mnras/stab1666](https://doi.org/10.1093/mnras/stab1666)
- Foreman-Mackey, D., Hogg, D. W., Lang, D., & Goodman, J. 2013a, PASP, 125, 306, doi: [10.1086/670067](https://doi.org/10.1086/670067)
- . 2013b, PASP, 125, 306, doi: [10.1086/670067](https://doi.org/10.1086/670067)
- Gaia Collaboration, Vallenari, A., Brown, A. G. A., et al. 2023, A&A, 674, A1, doi: [10.1051/0004-6361/202243940](https://doi.org/10.1051/0004-6361/202243940)
- Greene, J. E., & Ho, L. C. 2005, ApJ, 630, 122, doi: [10.1086/431897](https://doi.org/10.1086/431897)
- Heckman, T. M., Lehnert, M. D., Strickland, D. K., & Armus, L. 2000, ApJS, 129, 493, doi: [10.1086/313421](https://doi.org/10.1086/313421)
- Hickox, R. C., Mullaney, J. R., Alexander, D. M., et al. 2014, ApJ, 782, 9, doi: [10.1088/0004-637X/782/1/9](https://doi.org/10.1088/0004-637X/782/1/9)
- Hopkins, P. F., Hernquist, L., Martini, P., et al. 2005, ApJL, 625, L71, doi: [10.1086/431146](https://doi.org/10.1086/431146)
- Hopkins, P. F., Kereš, D., Oñorbe, J., et al. 2014, MNRAS, 445, 581, doi: [10.1093/mnras/stu1738](https://doi.org/10.1093/mnras/stu1738)
- Horne, K. 1986, PASP, 98, 609, doi: [10.1086/131801](https://doi.org/10.1086/131801)
- Inami, H., Bacon, R., Brinchmann, J., et al. 2017, A&A, 608, A2, doi: [10.1051/0004-6361/201731195](https://doi.org/10.1051/0004-6361/201731195)
- Jakobsen, P., Ferruit, P., Alves de Oliveira, C., et al. 2022, A&A, 661, A80, doi: [10.1051/0004-6361/202142663](https://doi.org/10.1051/0004-6361/202142663)
- Ji, Z., Williams, C. C., Tacchella, S., et al. 2024, ApJ, 974, 135, doi: [10.3847/1538-4357/ad6e7f](https://doi.org/10.3847/1538-4357/ad6e7f)
- Johnson, B. D., Leja, J., Conroy, C., & Speagle, J. S. 2021, ApJS, 254, 22, doi: [10.3847/1538-4365/abef67](https://doi.org/10.3847/1538-4365/abef67)
- Kauffmann, G., Heckman, T. M., Tremonti, C., et al. 2003, MNRAS, 346, 1055, doi: [10.1111/j.1365-2966.2003.07154.x](https://doi.org/10.1111/j.1365-2966.2003.07154.x)
- Kereš, D., Katz, N., Fardal, M., Davé, R., & Weinberg, D. H. 2009, MNRAS, 395, 160, doi: [10.1111/j.1365-2966.2009.14541.x](https://doi.org/10.1111/j.1365-2966.2009.14541.x)
- Kewley, L. J., Dopita, M. A., Sutherland, R. S., Heisler, C. A., & Trevena, J. 2001, ApJ, 556, 121, doi: [10.1086/321545](https://doi.org/10.1086/321545)
- Kewley, L. J., Maier, C., Yabe, K., et al. 2013, ApJL, 774, L10, doi: [10.1088/2041-8205/774/1/L10](https://doi.org/10.1088/2041-8205/774/1/L10)
- King, A., & Pounds, K. 2015, ARA&A, 53, 115, doi: [10.1146/annurev-astro-082214-122316](https://doi.org/10.1146/annurev-astro-082214-122316)
- Kroupa, P. 2001, MNRAS, 322, 231, doi: [10.1046/j.1365-8711.2001.04022.x](https://doi.org/10.1046/j.1365-8711.2001.04022.x)
- Leitherer, C., Schaerer, D., Goldader, J. D., et al. 1999, ApJS, 123, 3, doi: [10.1086/313233](https://doi.org/10.1086/313233)
- Leja, J., Carnall, A. C., Johnson, B. D., Conroy, C., & Speagle, J. S. 2019, ApJ, 876, 3, doi: [10.3847/1538-4357/ab133c](https://doi.org/10.3847/1538-4357/ab133c)
- Leja, J., Johnson, B. D., Conroy, C., van Dokkum, P. G., & Byler, N. 2017, ApJ, 837, 170, doi: [10.3847/1538-4357/aa5ffe](https://doi.org/10.3847/1538-4357/aa5ffe)
- Leja, J., Speagle, J. S., Ting, Y.-S., et al. 2022, ApJ, 936, 165, doi: [10.3847/1538-4357/ac887d](https://doi.org/10.3847/1538-4357/ac887d)
- Liu, T., Tozzi, P., Wang, J.-X., et al. 2017, ApJS, 232, 8, doi: [10.3847/1538-4365/aa7847](https://doi.org/10.3847/1538-4365/aa7847)
- Luo, B., Brandt, W. N., Xue, Y. Q., et al. 2017, ApJS, 228, 2, doi: [10.3847/1538-4365/228/1/2](https://doi.org/10.3847/1538-4365/228/1/2)
- Luo, Y., Rowlands, K., Alatalo, K., et al. 2022, ApJ, 938, 63, doi: [10.3847/1538-4357/ac8b7d](https://doi.org/10.3847/1538-4357/ac8b7d)
- Lyu, J., Alberts, S., Rieke, G. H., & Rujopakarn, W. 2022, ApJ, 941, 191, doi: [10.3847/1538-4357/ac9e5d](https://doi.org/10.3847/1538-4357/ac9e5d)
- Lyu, J., Alberts, S., Rieke, G. H., et al. 2024, ApJ, 966, 229, doi: [10.3847/1538-4357/ad3643](https://doi.org/10.3847/1538-4357/ad3643)
- Madau, P. 1995, ApJ, 441, 18, doi: [10.1086/175332](https://doi.org/10.1086/175332)
- Maltby, D. T., Almaini, O., McLure, R. J., et al. 2019, MNRAS, 489, 1139, doi: [10.1093/mnras/stz2211](https://doi.org/10.1093/mnras/stz2211)
- Naab, T., & Ostriker, J. P. 2017, ARA&A, 55, 59, doi: [10.1146/annurev-astro-081913-040019](https://doi.org/10.1146/annurev-astro-081913-040019)
- Netzer, H. 2009, MNRAS, 399, 1907, doi: [10.1111/j.1365-2966.2009.15434.x](https://doi.org/10.1111/j.1365-2966.2009.15434.x)
- . 2019, MNRAS, 488, 5185, doi: [10.1093/mnras/stz2016](https://doi.org/10.1093/mnras/stz2016)
- Neufeld, C., van Dokkum, P., Asali, Y., et al. 2024, ApJ, 972, 156, doi: [10.3847/1538-4357/ad6158](https://doi.org/10.3847/1538-4357/ad6158)
- Newville, M., Stensitzki, T., Allen, D. B., & Ingargiola, A. 2014, LMFIT: Non-Linear Least-Square Minimization and Curve-Fitting for Python, 0.8.0, Zenodo, doi: [10.5281/zenodo.11813](https://doi.org/10.5281/zenodo.11813)
- Noll, S., Burgarella, D., Giovannoli, E., et al. 2009, A&A, 507, 1793, doi: [10.1051/0004-6361/200912497](https://doi.org/10.1051/0004-6361/200912497)
- Oesch, P., & Magee, D. 2023, The JWST FRESCO Survey, STScI/MAST, doi: [10.17909/GDYC-7G80](https://doi.org/10.17909/GDYC-7G80)
- Oesch, P. A., Brammer, G., Naidu, R. P., et al. 2023, MNRAS, 525, 2864, doi: [10.1093/mnras/stad2411](https://doi.org/10.1093/mnras/stad2411)
- Osterbrock, D. E., & Ferland, G. J. 2006, Astrophysics of gaseous nebulae and active galactic nuclei
- Park, M., Belli, S., Conroy, C., et al. 2024, ApJ, 976, 72, doi: [10.3847/1538-4357/ad7e15](https://doi.org/10.3847/1538-4357/ad7e15)
- Pennell, A., Runnoe, J. C., & Brotherton, M. S. 2017, MNRAS, 468, 1433, doi: [10.1093/mnras/stx556](https://doi.org/10.1093/mnras/stx556)
- Perrotta, S., George, E. R., Coil, A. L., et al. 2021, ApJ, 923, 275, doi: [10.3847/1538-4357/ac2fa4](https://doi.org/10.3847/1538-4357/ac2fa4)
- Rafelski, M., Teplitz, H. I., Gardner, J. P., et al. 2015, AJ, 150, 31, doi: [10.1088/0004-6256/150/1/31](https://doi.org/10.1088/0004-6256/150/1/31)
- Rieke, G. H., Alberts, S., Shivaee, I., et al. 2024, ApJ, 975, 83, doi: [10.3847/1538-4357/ad6cd2](https://doi.org/10.3847/1538-4357/ad6cd2)
- Rieke, M., Robertson, B., Tacchella, S., et al. 2023a, Data from the JWST Advanced Deep Extragalactic Survey (JADES), STScI/MAST, doi: [10.17909/8TDJ-8N28](https://doi.org/10.17909/8TDJ-8N28)

- Rieke, M. J., Robertson, B., Tacchella, S., et al. 2023b, *ApJS*, 269, 16, doi: [10.3847/1538-4365/acf44d](https://doi.org/10.3847/1538-4365/acf44d)
- Rieke, George, Alberts, Stacey, Lyu, Jianwei, & Shivaiei, Irene. 2024, Systematic Mid-infrared Instrument Legacy Extragalactic Survey (SMILES), STScI/MAST, doi: [10.17909/ET3F-ZD57](https://doi.org/10.17909/ET3F-ZD57)
- Rupke, D. S., Veilleux, S., & Sanders, D. B. 2005a, *ApJS*, 160, 87, doi: [10.1086/432886](https://doi.org/10.1086/432886)
- . 2005b, *ApJ*, 632, 751, doi: [10.1086/444451](https://doi.org/10.1086/444451)
- . 2005c, *ApJS*, 160, 115, doi: [10.1086/432889](https://doi.org/10.1086/432889)
- Rupke, D. S. N. 2018, *Galaxies*, 6, 138, doi: [10.3390/galaxies6040138](https://doi.org/10.3390/galaxies6040138)
- Rupke, D. S. N., & Veilleux, S. 2015, *ApJ*, 801, 126, doi: [10.1088/0004-637X/801/2/126](https://doi.org/10.1088/0004-637X/801/2/126)
- Salpeter, E. E. 1955, *ApJ*, 121, 161, doi: [10.1086/145971](https://doi.org/10.1086/145971)
- Sánchez-Blázquez, P., Peletier, R. F., Jiménez-Vicente, J., et al. 2006, *MNRAS*, 371, 703, doi: [10.1111/j.1365-2966.2006.10699.x](https://doi.org/10.1111/j.1365-2966.2006.10699.x)
- Silva-Lima, L. A., Martins, L. P., Coelho, P. R. T., & Gadotti, D. A. 2022, *A&A*, 661, A105, doi: [10.1051/0004-6361/202142432](https://doi.org/10.1051/0004-6361/202142432)
- Somerville, R. S., & Davé, R. 2015, *ARA&A*, 53, 51, doi: [10.1146/annurev-astro-082812-140951](https://doi.org/10.1146/annurev-astro-082812-140951)
- Steidel, C. C., Erb, D. K., Shapley, A. E., et al. 2010, *ApJ*, 717, 289, doi: [10.1088/0004-637X/717/1/289](https://doi.org/10.1088/0004-637X/717/1/289)
- Sun, F. 2024, nircam_grism, Zenodo, doi: [10.5281/ZENODO.14052875](https://doi.org/10.5281/ZENODO.14052875)
- Sun, F., Egami, E., Pirzkal, N., et al. 2023, *ApJ*, 953, 53, doi: [10.3847/1538-4357/acd53c](https://doi.org/10.3847/1538-4357/acd53c)
- Sun, Y., Lee, G.-H., Zabludoff, A. I., et al. 2024, *MNRAS*, 528, 5783, doi: [10.1093/mnras/stae366](https://doi.org/10.1093/mnras/stae366)
- Sun, Y., Lyu, J., Rieke, G. H., et al. 2025, *ApJ*, 978, 98, doi: [10.3847/1538-4357/ad973b](https://doi.org/10.3847/1538-4357/ad973b)
- Taylor, E., Maltby, D., Almaini, O., et al. 2024, *MNRAS*, 535, 1684, doi: [10.1093/mnras/stae2463](https://doi.org/10.1093/mnras/stae2463)
- Tremonti, C. A., Moustakas, J., & Diamond-Stanic, A. M. 2007, *ApJL*, 663, L77, doi: [10.1086/520083](https://doi.org/10.1086/520083)
- Veilleux, S., Cecil, G., & Bland-Hawthorn, J. 2005, *ARA&A*, 43, 769, doi: [10.1146/annurev.astro.43.072103.150610](https://doi.org/10.1146/annurev.astro.43.072103.150610)
- Veilleux, S., & Osterbrock, D. E. 1987, in *NASA Conference Publication*, Vol. 2466, NASA Conference Publication, ed. C. J. Lonsdale Persson, 737–740
- Virtanen, P., Gommers, R., Oliphant, T. E., et al. 2020, *Nature Methods*, 17, 261, doi: [10.1038/s41592-019-0686-2](https://doi.org/10.1038/s41592-019-0686-2)
- Weiner, B. J., Coil, A. L., Prochaska, J. X., et al. 2009, *ApJ*, 692, 187, doi: [10.1088/0004-637X/692/1/187](https://doi.org/10.1088/0004-637X/692/1/187)
- Wu, P.-F. 2025, *ApJ*, 978, 131, doi: [10.3847/1538-4357/ad98ef](https://doi.org/10.3847/1538-4357/ad98ef)
- Zhu, Y., Rieke, M. J., Ji, Z., et al. 2024a, arXiv e-prints, arXiv:2409.11464, doi: [10.48550/arXiv.2409.11464](https://doi.org/10.48550/arXiv.2409.11464)
- Zhu, Y., Alberts, S., Lyu, J., et al. 2024b, arXiv e-prints, arXiv:2410.14804, doi: [10.48550/arXiv.2410.14804](https://doi.org/10.48550/arXiv.2410.14804)
- Zubovas, K., Bialopetravičius, J., & Kazlauskaitė, M. 2022, *MNRAS*, 515, 1705, doi: [10.1093/mnras/stac1887](https://doi.org/10.1093/mnras/stac1887)
- Zubovas, K., & Nardini, E. 2020, *MNRAS*, 498, 3633, doi: [10.1093/mnras/staa2652](https://doi.org/10.1093/mnras/staa2652)